UNIVERSIDADE DE SÃO PAULO
ESCOLA DE ENGENHARIA DE SÃO CARLOS

KATHERINE SANTOS OLIVEIRA

Phase characterization in crystallized glasses in the $Na_2O.2CaO.3SiO_2$-$Na_2O.3CaO.6SiO_2$ pseudo-binary system

São Carlos
2021

KATHERINE SANTOS OLIVEIRA

Phase characterization in crystallized glasses in the $Na_2O.2CaO.3SiO_2$-$Na_2O.3CaO.6SiO_2$ pseudo-binary system

VERSÃO CORRIGIDA

Dissertação apresentada ao programa de Pós-Graduação em Ciência e Engenharia de Materiais da Universidade de São Paulo, para obtenção do título de Mestre em Ciências

Área de Concentração: Desenvolvimento, Caracterização e Aplicação de Materiais

Orientador: Prof. Dr. Eduardo Bellini Ferreira

São Carlos

2021

Ficha catalográfica elaborada pela Biblioteca Prof. Dr. Sérgio Rodrigues Fontes da EESC/USP com os dados inseridos pelo(a) autor(a).

Oliveira, Katherine Santos
O48p Phase characterization in crystallized glasses in the Na2O.2CaO.3SiO2-Na2O.3CaO.6SiO2 pseudo-binary system / Katherine Santos Oliveira; orientador Eduardo Bellini Ferreira. São Carlos, 2021.

Dissertação (Mestrado) - Programa de Pós-Graduação em Ciência e Engenharia de Materiais e Área de Concentração em Desenvolvimento, Caracterização e Aplicação de Materiais -- Escola de Engenharia de São Carlos da Universidade de São Paulo, 2021.

1. Vidros. 2. Vitrocerâmicas. 3. Cristalização. 4. Solução sólida. I. Título.

Eduardo Graziosi Silva - CRB - 8/8907

FOLHA DE JULGAMENTO

Candidata: Engenheira **KATHERINE SANTOS OLIVEIRA.**

Título da dissertação: "Caracterização de fases em vidros cristalizados no sistema Na2O.2CaO.3SiO2-Na2O.3CaO.6SiO2".

Data da defesa: 10/12/2021.

Comissão Julgadora	**Resultado**
Prof. Dr. **Eduardo Bellini Ferreira** **(Orientador)** (Escola de Engenharia de São Carlos/EESC-USP)	Aprovado
Prof. Dr. **Murilo Camuri Crovace** (Universidade Federal de São Carlos/UFSCar)	Aprovado
Prof. Dr. **Raphael Midea Cuccovia Vasconcelos Reis** (Universidade Federal Fluminense/UFF)	Aprovado

Coordenador do Programa de Pós-Graduação em Engenharia de Materiais:
Prof. Associado **Rafael Salomão**

Presidente da Comissão de Pós-Graduação:
Prof. Titular **Murilo Araujo Romero**

DEDICATÓRIA

A meu avô Antonio Alves dos Santos.

AGREDECIMENTOS

Ao Prof. Vladimir Mikhailovich Fokin pela contribuição ímpar no desenvolvimento deste trabalho.

Ao Prof. Eduardo Bellini Ferreira pela orientação e paciência durante os últimos anos.

A meus pais, Paulo Roberto de Oliveira e Cleide dos Santos Oliveira, meus avós, Antonio Alves dos Santos e Marina Vieira dos Santos e meu companheiro Manuel Silva Zurita pelo amor e apoio em todos os momentos.

Aos meus amigos Guilherme e Carolina pelos ensinamentos e momentos de descontração.

Ao Prof. Valmor Roberto Mastelaro pelo auxílio no trabalho experimental.

Aos funcionários e docentes do Departamento de Engenharia de Materiais da Escola de São Carlos (SMM-EESC/USP).

Ao CNPq pelo fomento deste projeto de mestrado (Projeto: 830729/1999-2).

RESUMO

OLIVEIRA, K. S. **Caracterização de fases em vidros cristalizados no sistema $Na_2O.2CaO.3SiO_2$-$Na_2O.3CaO.6SiO_2$, 2021.** 84 pg. Dissertação (Mestrado) – Escola de Engenharia de São Carlos, Universidade de São Paulo, São Carlos, 2021.

As vitrocerâmicas possuem grande relevância na indústria devido à ampla variedade de utilizações. Suas propriedades resultam do controle rigoroso da microestrutura durante a cristalização do vidro precursor. O sistema Na_2O-CaO-SiO_2 é de grande interesse na indústria do vidro, encontrando aplicações desde janelas convencionais e embalagens até biovidros usados na medicina, entre vários outros. A cinética de cristalização de composições estequiométricas neste sistema foi extensivamente estudada. No entanto, há uma falta de informações sobre as fases cristalizadas no sistema pseudo-binário combeíta-devitrita ($Na_2O{\cdot}2CaO{\cdot}SiO_2$-$Na_2O{\cdot}3CaO{\cdot}6SiO_2$). Neste trabalho, a formação de fase em composições estequiométricas e não estequiométricas na junção pseudo-binária combeíta-devitrita foi investigada por difração de raios X (XRD), calorimetria diferencial de varredura (DSC), microscopia óptica e microscopia eletrônica de varredura (MEV). A combeíta foi a primeira fase cristalizada em todos os vidros de composições não estequiométricas tratados perto da temperatura de início da cristalização (cerca de 750 ° C) determinada por DSC. Em um vidro de composição eutética (33,3 mol% devitrita), devitrita foi observada apenas acima de 810 ° C, em estágios avançados de cristalização. A formação de devitrita foi acompanhada por uma diminuição na fração de volumétrica da solução sólida de combeíta. Em contraste, em uma composição hipereutética (50 mol% de devitrita), cristais de devitrita nuclearam heterogeneamente a partir da superfície da camada de combeíta. A decomposição da devitrita em wolastonita e líquido ocorreu acima de 1050 ° C para vidros com composições entre 33,33 e 93,75 mol% de devitrita. Apenas vidros na seção hipoeutética do sistema binário combeíta - devitrita apresentaram nucleação homogênea. Para essas composições, a formação de solução sólida de combeíta foi investigada por XRD. Sugere-se que combeíta em solução sólida ocorra no intervalo entre 0 e 33,33 mol% de devitrita. Essas descobertas são relevantes para aplicações teóricas e práticas.

Palavras-chave: Vidros. Vitrocerâmicas. Cristalização. Solução Sólida.

ABSTRACT

OLIVEIRA, K. S. **Phase characterization in crystallized glasses in the $Na_2O.2CaO.3SiO_2$-$Na_2O.3CaO.6SiO_2$ pseudo-binary system., 2021.** 84 pg. Dissertation (Master of Science) – Escola de Engenharia de São Carlos, Universidade de São Paulo, São Carlos, 2021.

Glass-ceramics are of the highest relevance in the industry due to their wide variety of uses. Compared to their parent glass, their enhanced properties result from the rigorous microstructure control during the precursor glass crystallization. Remarkably, the Na2O-CaO-SiO2 system is of great interest in the glass industry, finding applications from conventional windows, packaging, and tableware to bioglasses in medicine, among several others. The crystallization kinetics of stoichiometric compositions in this system has been extensively studied. However, there is a lack of information on the phases crystallized in the combeite-devitrite (Na2O·2CaO·3SiO2-Na2O·3CaO·6SiO2) pseudo-binary system. In this work, the phase formation in stoichiometric and non-stoichiometric compositions in the combeite-devitrite pseudo-binary join was investigated by X-ray diffraction (XRD), differential scanning calorimetry (DSC), optical microscopy and, scanning electron microscopy (SEM). In moderate undercooling below the liquidus, combeite was the primary phase crystallizing in all glasses of non-stoichiometric compositions treated close to the temperature of crystallization onset (about 750 °C) determined by DSC. In a glass of eutectic composition (33.3 mol% devitrite), the devitrite was observed only above 810 °C in advanced stages of crystallization. The devitrite formation was accompanied by a decrease in the volume fraction of the combeite solid solution. In contrast, in a hyper-eutectic composition (50 mol% devitrite), devitrite nucleated heterogeneously and grew from the surface of combeite crystals immediately after the combeite formation. The decomposition of devitrite into wollastonite and liquid occurred above 1050 °C for glasses with compositions between 33.33 and 93.75 mol% devitrite. Only glasses in the hypo-eutectic section of the combeite-devitrite binary system presented homogeneous nucleation. For these compositions, the combeite solid solution formation was investigated by XRD. It is suggested that combeite solid solution occurs in the interval between 0 and 33.33 mol% devitrite. The microstructure assessment in glass-ceramics from combeite-devitrite pseudo-binary glass compositions sheds light on the phase formation in this system, which is relevant for theoretical and practical applications.

Keywords: Glass. Glass-ceramic. Crystallization. Solid solution.

LISTA DE ILUSTRAÇÕES

LISTA DE TABELAS

SUMMARY

1 INTRODUCTION

Glasses are non-crystalline materials that behave like solids in several aspects, but with an amorphous atomic structure, similar to liquids, although frozen in respect to observable time. When subjected to appropriate heat treatments, these materials can have their properties changed by crystallization. This process consists primarily of two overlapped stages, nucleation and crystal growth, and when one manages to get good properties for a given use, the resulting material is called glass-ceramic. Among the commercially available glasses, the soda-lime silicates are of the highest relevance due to their wide range of applications, from windows to bioactive implants for medical purposes, abundance and low price of raw materials used in their fabrication. Unlike most glasses, some with compositions in the soda-lime-silica system present homogeneous nucleation, which can lead to glass-ceramics by volume crystallization.

It is necessary to determine the glass crystallization kinetics to design glass-ceramics microstructures properly. Despite the fact that most glass-ceramics have nonstoichiometric compositions, the first studies on the crystallization kinetics of glasses in the Na_2O-CaO-SiO_2 system investigated only stoichiometric compositions [1,2]. After, Fokin *et al.* [3,4] and Soboleva *et al.* [5] studied the crystallization kinetics of nonstoichiometric glasses in the Na_2SiO_3–$CaSiO_3$ pseudo-binary join, whose crystal compositions were sodium-enriched solid solutions based on combeite ($Na_2O{\cdot}2CaO{\cdot}3SiO_2$), of general formula $Na_{4+2x}Ca_{4-x}[Si_6O_{18}]$ ($0 \leq x \leq 1$) [4]. In [4], Fokin *et al.* reported the existence of combeite crystals with the composition varying along their diameter in stoichiometric $Na_2O{\cdot}2CaO{\cdot}3SiO_2$ glass and compositions close to it. Sodium-enriched nuclei of combeite formed in isothermally treated glasses and, as crystallization proceeded, the composition of the crystal approaches that of the parent glass due to the reduction of the concentration of Na cations in the residual glass. The precipitation of metastable combeite solid solution reduces the thermodynamical barrier to nucleation by decreasing the surface energy between the crystal and the liquid.

In recent work, Macena *et al* [6,7] studied the kinetics of crystallization of glasses in the $Na_2O{\cdot}2CaO{\cdot}3SiO_2$–$Na_2O{\cdot}3CaO{\cdot}6SiO_2$ join. This author reported that combeite was the only phase observed in the volume of glasses containing less than 33.3 mol% of devitrite. The compositional profile of combeite crystals was also investigated as a dependence of crystallized volume fraction. It was concluded that combeite solid solution enriched in Na^+ was crystallized.

Thus, this work aims to advance the study of combeite solid solutions in the $Na_2O{\cdot}2CaO{\cdot}3SiO_2$–$Na_2O{\cdot}3CaO{\cdot}6SiO_2$ binary system. It was reported in [6] a change in the thermal effects observed in DSC curves from the eutectic (33.33 mol% devitrite) towards stoichiometric devitrite of the pseudo-binary. Therefore, the phase formation in compositions 33.3 and 50 mol% of devitrite were investigated. Moreover, the characteristic temperatures of glasses in this system were measured to complete previous diagram phase data obtained by [6]. Thermal analysis, XRD, optical microscopy and, SEM were the main techniques used in this research.

2 THEORETICAL BACKGROUND

2.1 Definition of glass

Glasses can be explained in terms of their structural and thermodynamic properties as off-equilibrium and non-crystalline materials that do not present long- or medium-distance order in the three-dimensional atomic structure and exhibit the glass transition phenomenon [8]. They are produced under specific conditions to prevent crystallization on cooling from the liquid. Thus, the most common fabrication technique consists of cooling a melt at a rate fast enough. However, since a perfectly amorphous structure is unlikely to be reached by this process, a critical cooling rate for glass forming, CCR, is defined to yield a maximum crystallized volume fraction of 10^{-2}-10^{-6}, given by the resolution limit of some experimental technique.

The crystalline solid is the thermodynamically stable state of matter below the melting temperature, T_m, or the solidus for incongruent melting compositions. However, at relatively fast cooling rates, a metastable state defined as a supercooled liquid, SCL, can be reached (Figure 1). As the temperature decreases, the atoms in the SCL gradually lose mobility due to the reduction in diffusion rate (by viscous flow or another mechanism), reaching a temperature range one no longer observes the relaxation to the reference structure, namely the glass transition range. In other words, in this temperature range, which depends on the cooling rate, the experimental time of observation, t_{obs}, is of the same order of magnitude as the time of structural relaxation, τ. Below it, the structure no longer relaxes and freezes relatively to the human observation time, and the material becomes a glass [8]. Since the glass transition is a kinetic phenomenon, T_g depends on the cooling rate. For oxide glasses in laboratory experiments, T_g may be defined as the temperature at which the viscosity is about 10^{12} Pa.s [9,10].

The glass transition is characterized by a change in the derivative of the temperature function of some thermodynamic property, for instance, the enthalpy (Figure 1). On the other hand, the liquid-crystal transformation is described by a discontinuity in such properties. It is worth noting that the transition of SCL into a glass is not a phase transformation since this process does not involve any change in atomic structure or composition.

Figure 1: Thermodynamic property as a function of the temperature.

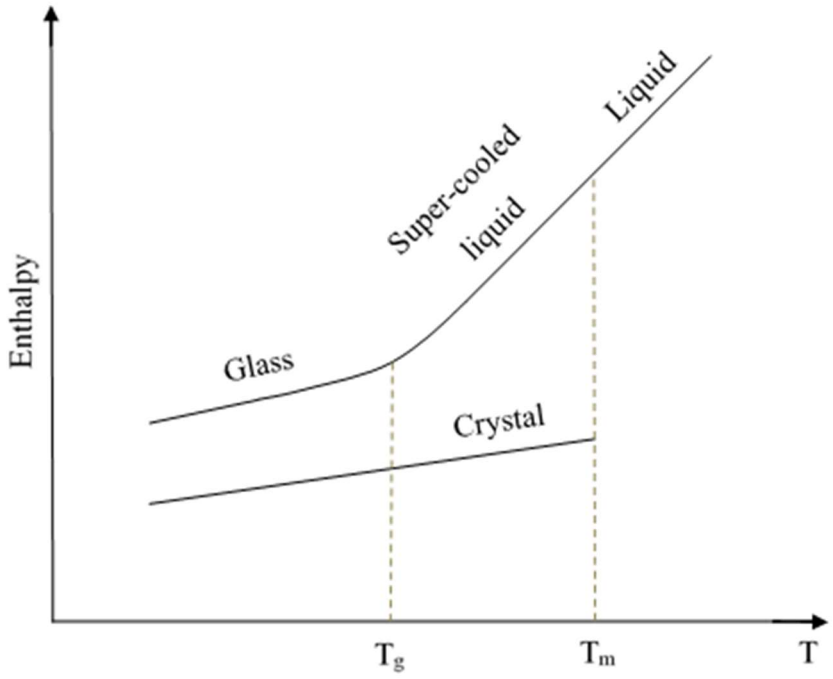

Source: Author (2021)

2.2 Nucleation and growth

Glasses are thermodynamically unstable related to the SCL at a given temperature [8]. The glass-SCL transformation is a spontaneous process at which the glass structure relaxes towards the SCL and only depends on the system kinetics. When the glass is at a temperature above the glass transition temperature, structural relaxation immediately begins towards the structure of the metastable supercooled liquid. The nucleation process coincides with this structural relaxation and depends on it as the structure changes. Thus, nucleation begins in glass, continues in a changing supercooled liquid, and then in a metastable equilibrium SCL [11–13].

Controlling the crystallization in glasses makes it possible to obtain a polycrystalline material with improved mechanical properties, such as strength and toughness, besides transparency, and a low or null thermal expansion coefficient. [14]. Also, the so-called glass-ceramics produced by this process can have nearly zero or null porosity. As a further advantage, the final processing temperatures are lower than in the traditional ceramic fabrication process by sintering. Glass-ceramics are characterized by a fine and homogeneous microstructure and find use in a wide range of applications since their properties can be designed to meet rigorous specifications [15].

Thus, the precise control of glass crystallization is of great interest in glass science and technology and is a consequence of a continuous process comprised of nucleation and crystal growth driven by thermodynamic and kinetic phenomena.

2.2.1 Nucleation

Below T_m, the thermodynamically stable phase is crystalline. Its free energy, G_c, is lower than the liquid's G_l. The system free-energy change $\Delta G = G_c - G_l < 0$ is the driving force for crystallization.

The atoms in the SCL undergo localized position fluctuations, eventually grouping into clusters with a structure similar to that of the crystalline phase. Once these clusters, or embryos, reach a critical size, r^*, they grow to form a stable phase. Otherwise, they can dissolve. The volumetric free energy, ΔG_V, associated with this local ordering is negative. Consequently, as the embryo grows, ΔG decreases. However, the system energy increases with the creation of the new liquid/crystal interface. The work, G, needed to form a spherical embryo as a function of the radius, r, and temperature is described by Eq. 1 [11]:

$$\mathbf{G(r,T) = 4\pi r^2\,\sigma_{cl} + \frac{4\pi}{3}\,r^3\,\Delta G_V\,(T)} \tag{1}$$

where, σ_{cl} is the liquid-crystal surface energy, $\Delta G_V = \Delta G / V_m$, and V_m is the molar volume. The behavior given by Eq. (1) is shown in Figure 2. In the early stages, the surface to volume ratio is high, causing the embryo to be unstable since the surface energy exceeds the volumetric free energy variation. For $r \geq r^*$, any increase in crystal volume decreases ΔG, the embryo becomes a stable nucleus and grows spontaneously.

The maximum of the curve described by Eq. (1) corresponds to the thermodynamic barrier to nucleation, W^*, given by Eq. (2).

$$W^*(T) = \frac{16\pi}{3}\frac{{\sigma_{cl}}^3}{\Delta G_V(T)^2} \tag{2}$$

It can be shown that r^* is given by:

$$r^*(T) = -2\frac{\sigma_{cl}}{\Delta G_V(T)} \tag{3}$$

According to the Classical Nucleation Theory (CNT), the nucleation rate at the steady-state regimen, I_{st}, is [16,17]:

$$I_{st} = I_o \exp\left[-\frac{W^* + \Delta G_D}{k_b T}\right] \quad (4)$$

where I_o is a pre-exponential parameter with values between 10^{41} to 10^{43} $m^3.s^{-1}$, ΔG_D is the activation free energy for the diffusion of nucleating block, and k_b is the Boltzmann constant [17]. As shown in Eq. (4), in addition to W^*, the crystal growth is also influenced by a diffusional or kinetic barrier, because atoms from the SCL need to get transported to the liquidus-nucleus interface to attach to the crystalline structure.

Figure 2: Free energy diagram showing the thermodynamic barrier to nucleation.

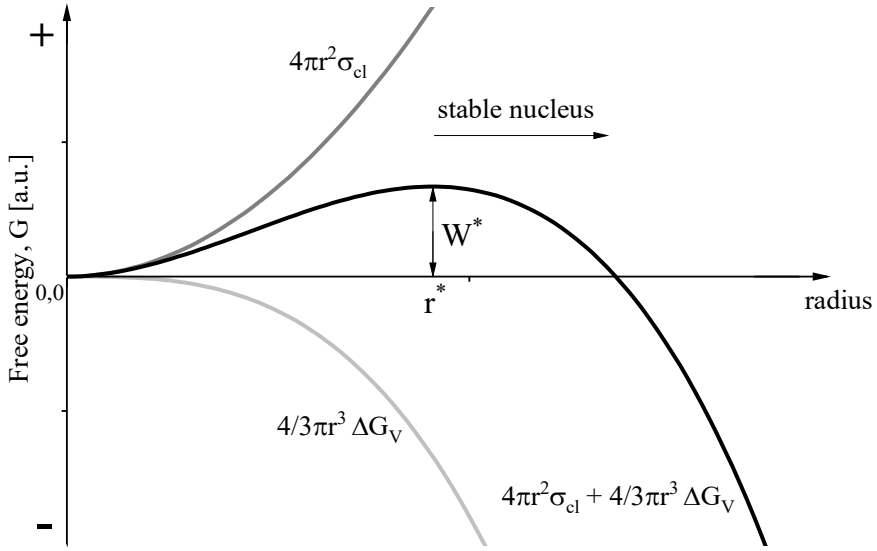

Source: Author (2021)

The process described above is known as homogeneous nucleation, in which the nuclei can form with the same probability in any region of the material volume. If the undercooling $\Delta T = T_m - T$ is small, the thermodynamic component in Eq. (4) controls nucleation. Consequently, the rate depends more strongly on ΔG_V. In contrast, at a low degree of undercooling, I_{st} is ruled by the transport factor, ΔG_D. Therefore, the nucleation rate as a function of temperature passes through a maximum between T_g and T_m. For a glass that nucleates homogeneously, the maximum nucleation rate occurs at approximately $T \sim 0.5 - 0.6\, T_m$ [18].

Heterogeneous nucleation occurs when there is nucleation in preferential sites. Here, the foreign surfaces, such as impurities and pores, do not affect the volume free energy and the

diffusion energy coefficient. However, they can reduce the nuclei-SCL interface energy. As a general effect, nucleation is catalyzed at lower undercooling by the reduced thermodynamic barrier. Despite the change in the surface energy, the mechanism of heterogeneous nucleation is analogous to the homogeneous one and is given by [17]:

$$I_{st,het}(T) = N_s \frac{k_b T}{h} \exp\left[-\frac{W^*(T)\phi + \Delta G_D(T)}{k_b T}\right] \quad (5)$$

where N_s is the number of heterogeneous nucleation sites, ϕ is a parameter between 0 and 1, and h is the Plank constant. Since few glass compositions undergo homogeneous nucleation, catalyst nucleating agents are added to promote volume crystallization [19], which behave as heterogeneous nucleation sites of the desired crystalline phase.

The surface crystallization at the air-glass interface is a particular case of heterogeneous nucleation. In general, the nucleation rate involved in this process is very high compared to the number of available sites for nucleation. The formation of new nuclei takes place up to a fixed number, and heterogeneous surface nucleation suddenly terminates [20]. Therefore, the number of nucleation sites per unit area, Ns, usually becomes practically constant during crystallization. In other words, it does not significantly depend on the temperature or time of heat treatment.

2.2.2 Crystal growth

After nuclei formation, the system's energy is further reduced by the increasing crystal volume (Figure 2). Since there is no thermodynamic barrier, the rate the crystals grow is determined by the speed at which the atoms arrive at the phase boundary and attach to the interface. The crystal growth rate, $u(T)$, is given as follows [21]:

$$u(T) = \frac{D_u}{\lambda}\left(1 - \exp\left(-\frac{\Delta G}{RT}\right)\right) \quad ((6)$$

where λ is the average distance between atoms in the liquid and the crystal's surface, D_u is the diffusion coefficient for crystal growth and R is the universal gas constant.

Similar to Eq. (4), Eq. (6) shows a maximum value. Crystal growth, differently of nucleation, is only associated with the transport of atoms to the crystal-liquid interface, which is represented by the first term D_u/λ in Eq. (6). At a high undercooling, this term diminishes with the increase of viscosity, whereas, the second factor $\left(1 - exp(-\Delta G/RT)\right)$ increases with the increase of driving force to crystallization, ΔG.

The resulting microstructures as crystal growth proceeds are shown in Figure 3. In Figure 3a, the glass undergoes internal crystallization. This process can derive from catalyst nucleating agents or homogeneous nucleation, leading to randomly oriented and uniformly dispersed crystals. In contrast, Figure 3b shows the microstructure for cases in which nucleation occurs at surface sites without volume nucleation. After the first step of crystallographic direction selection, the crystals grow with their fastest-growing axis perpendicular to the surface.

Figure 3: Schematic representation of a) volume and b) surface crystallization.

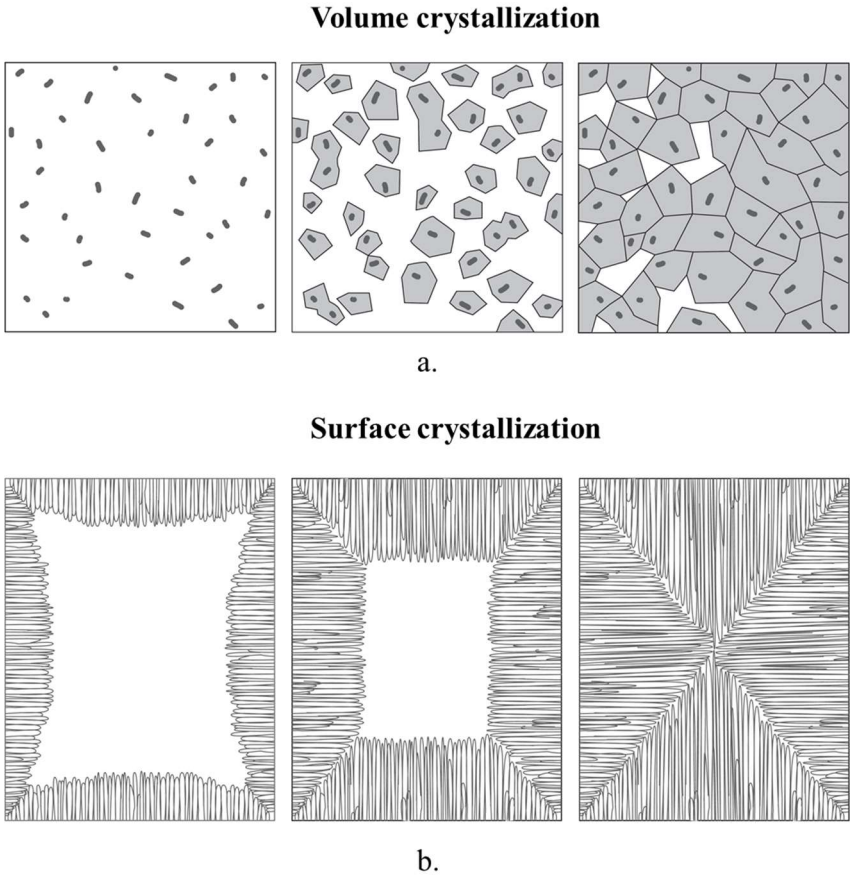

Source: Adapted from Höland and Beall (2012) [22]

2.3 The Na_2O-CaO-SiO_2 system

Soda-lime-silica compositions constitute most commercial glass products, such as windows, cookware, tableware, packaging for food and medicine [14,23,24], and promising materials for bioactive implants [6,25,26]. Also, the necessary raw materials to produce these glasses are abundant, non-toxic, and relatively non-expensive.

The crystallization kinetics of stoichiometric compositions in the Na_2O-CaO-SiO_2 system have been extensively studied. However, the crystallization kinetics of nonstoichiometric glasses in this system is not well known, despite their importance [4,6,27]. In this work, stoichiometric and non-stoichiometric compositions in the $Na_2O{\cdot}2CaO{\cdot}3SiO_2$-$Na_2O{\cdot}3CaO{\cdot}6SiO_2$ pseudo-binary join of the ternary Na_2O-CaO-SiO_2 system are investigated (Figure 4). This join includes in its ends two stoichiometric compositions, namely, combeite, $Na_2O{\cdot}2CaO{\cdot}3SiO_2$ (C), and devitrite, $Na_2O{\cdot}3CaO{\cdot}6SiO_2$ (D), which lies on the primary fields of combeite and wollastonite, $CaO{\cdot}SiO_2$ (CS), respectively. Combeite melts congruently melting at 1280 °C, while devitrite decomposes to wollastonite and liquid above 1030 °C. A eutectic close to 55.5 wt% SiO_2 (33.3 mol% D) at 1259 °C was confirmed [6,7].

Figure 4: Na_2O-CaO-SiO_2 phase diagram (weight %) showing highlighted (red) the join between the combeite ($Na_2O{\cdot}2CaO{\cdot}3SiO_2$) and devitrite ($Na_2O{\cdot}3CaO{\cdot}6SiO_2$).

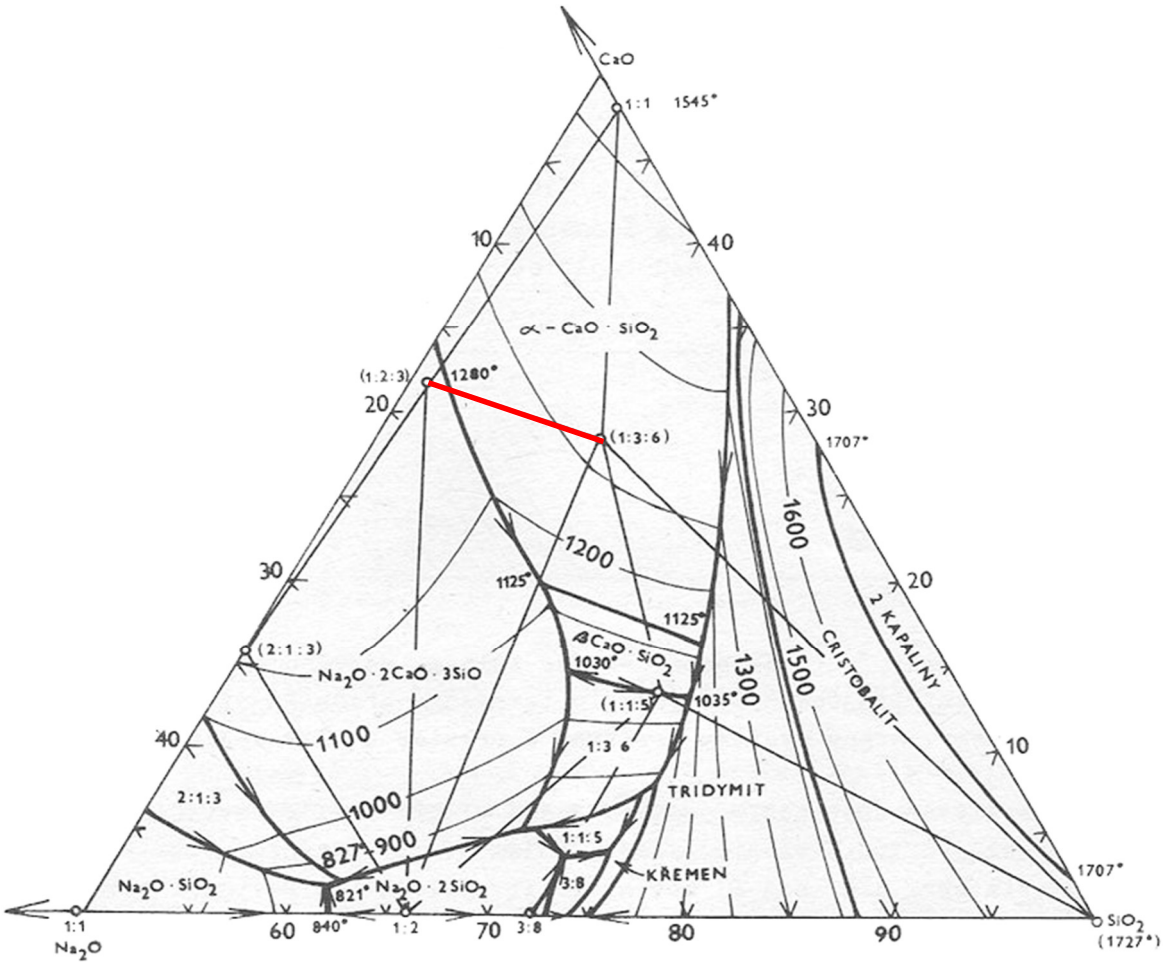

Source: Adapted from Shadid and Glasser (1972). [28]

Combeite belongs to the small group of glass compositions that exhibit homogeneous nucleation, i.e., nucleating agents are unnecessary to produce polycrystalline pieces by volume

crystallization of the glass. Figure 5 shows combeite crystals homogeneously nucleated in a composition of C-D pseudo-binary join. Encouraging results have shown that materials containing combeite can be applied as bioactive ceramics with improved toughness and mechanical strength [26]. In the soda-lime-silica system, combeite solid solution (C s.s.) was reported in $CaO{\cdot}SiO_2$-$Na_2O{\cdot}SiO_2$ [5,29] and $Na_2O{\cdot}2CaO{\cdot}3SiO_2$-$Na_2O{\cdot}3CaO{\cdot}6SiO_2$ [6,7] joins. The investigation of C s.s. formation and devitrite in the C-D system is one of the aims of this work and will be discussed in the following sections.

Figure 5: SEM image of combeite crystals.

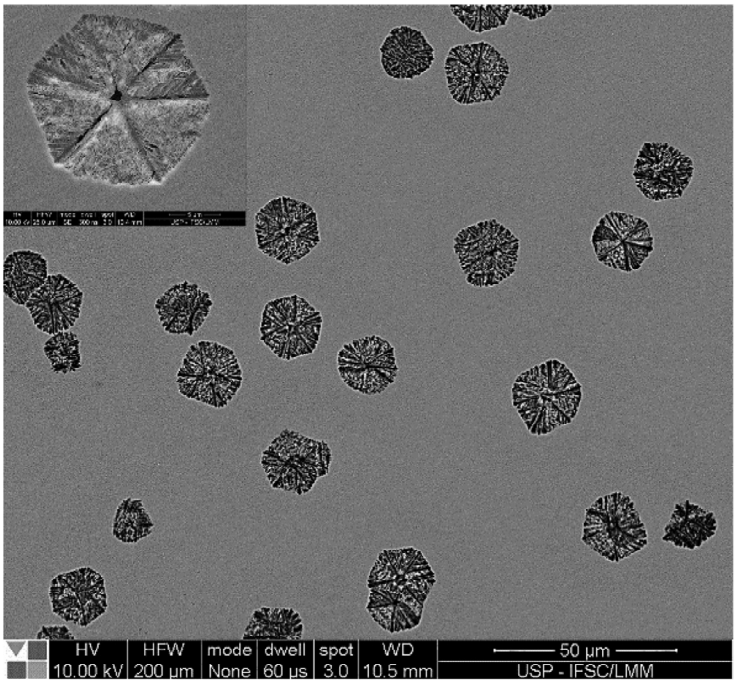

Source: Adapted from Macena *et al.* (2020) [7]

Devitrite was named after a typical phase in the devitrification of commercial glasses and is a natural product of the uncontrolled crystallization of soda-lime-silica glasses. The term "devitrification" is widely used in glass technology referring to the undesirable crystallization during fabrication [30]. Prolonged heat treatments can result in the heterogeneous crystallization of devitrite with lath-fan morphology on the surface of soda-lime-silica glasses (Figure 6)[31]. In general, devitrite nucleates on the glass surface and grows towards its center as needles bundles. The crystals grow along the [100] direction of the triclinic unit cell, giving this material interesting optical properties. Unfortunately, researchers lost interest in investigating it since the glass industry developed efficient techniques to avoid devitrite. However, recent studies reported low-cost optical diffusers based on the highly oriented acicular crystals of devitrite [32,33].

Figure 6: Polarized light optical micrography o fan of needles of devitrite.

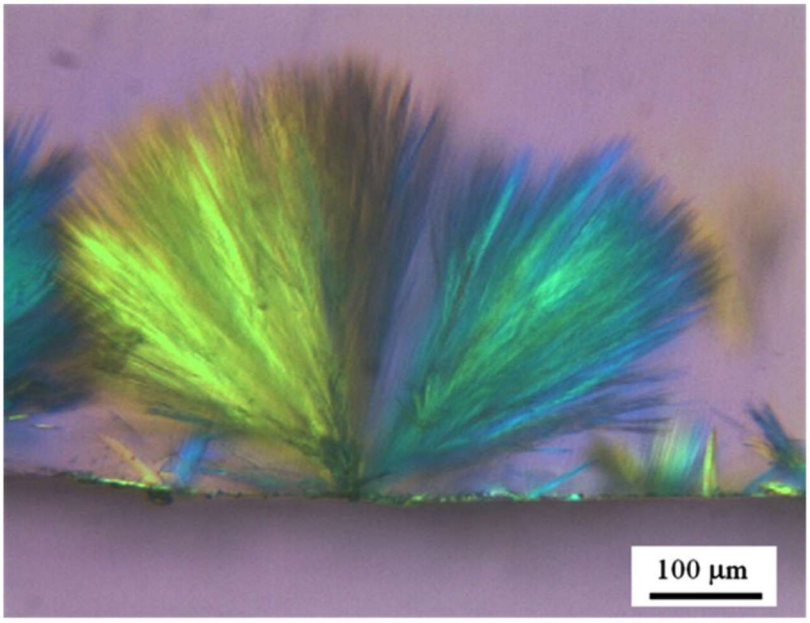

Source: Adapted from Knowles and Thompson (2014) [31]

Wollastonite can be used in biological implants and drug delivery [34,35]. Usually, the CS crystallization in glasses occurs from the surface. Its needle-like crystals can be designed to mimic the bone microstructure [36] and play a significant role in improving mechanical strength and biocompatibility [37]. There are three wollastonite polymorphs: wollastonite, para-wollastonite (β-CS), and pseudo-wollastonite (α-CS). At low temperatures, CS occurs as wollastonite (triclinic) and para-wollastonite (monoclinic), which are very similar in terms of microstructure. Above 1125 °C, wollastonite changes to pseudo-wollastonite, which melts at 1544 °C.

Figure 7: Optical micrography of acicular wollastonite crystals.

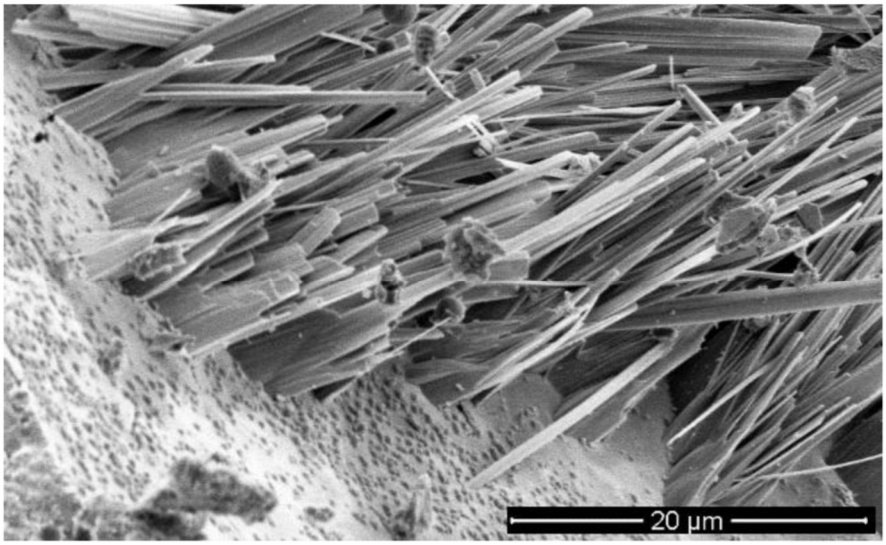

Source: Adapted from Nurjaya *et al.* (2015) [38]

3 Characteristics of the $Na_2O{\cdot}2CaO{\cdot}3SiO_2$ structure

Combeite exists in the form of two polymorphic phases: a high-temperature rhombohedral form and a low-temperature hexagonal form [29]. The transformation temperatures may be represented as follows:

$$\text{Hexagonal} \overset{485\,^{\circ}\text{C}}{\longleftrightarrow} \text{Rhombohedral} \overset{1280\,^{\circ}\text{C}}{\longrightarrow} \text{Melt} \tag{7}$$

Structurally, the high-temperature form is composed of puckered rings with six tetrahedra $[Si_6O_{18}]^{12-}$ (Figure 8a) arranged along the c axis in a cubic-close-packed fashion. Ca and Na cations are located in M1, M2, M3, and M4 sites and are shared between rings. Sites M1, M3 and M4 are occupied by cations (Na^+ and Ca^{2+}) and M2 sites by 2:1 Na^+ ions and vacancies. As shown in Figure 8b, on cooling below 485 °C, site M2 is transformed into M21, completely occupied by Na^+, and M22, vacant. Likewise M3 splits into M31, with 43% Na^+ and 57% Ca^{2+} ions, and M32 100% occupied by Ca^{2+}. Due to ring retraction and distortion of Si-O-Si angles, the sites M1 are divided into M1 and M1'.

The hexagonal and rhombohedral forms have the following sets of lattice parameters: $a = 10.471$ Å, $c = 13.174$ Å at room temperature; and $a = 7.53$ Å, $\alpha = 89°07'$, at 550 ℃. The relation between these crystalline phases is well discussed in the literature [39–41].

Figure 8: Perspective view of silicate rings of the structure of combeite projected along the trigonal c axis (a) High-temperature, and (b) low-temperature [39]

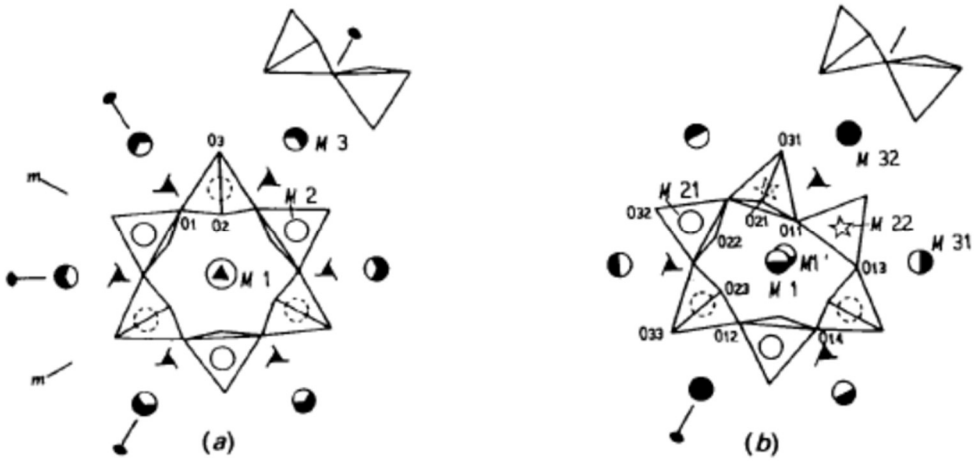

Source: Adapted from Ohsato *et al.* (1990) [39]

3.1 Solid solution

The inclusion of foreign atoms or ions in a crystalline lattice results either in a solid solution or a new phase, depending on the final system energy. A solid solution occurs when introducing atoms or solute reduces the system's free energy by substituting atoms from the host crystal or solvent or occupying interstitial sites. Here, the host crystal structure is maintained, although changes in the lattice parameters may occur according to the concentration of solute added [42]. On the other hand, if adding atoms increases the system energy, the solid solution will not be stable, and the components will split into new phases with different structures.

Often, there is a maximum concentration of solute at a given temperature, beyond which further addition of solute will cause the formation of another phase. In a phase diagram, this boundary is represented by the solvus line. Some mixtures of oxides can form solid solutions over the full range of components proportions, such as MgO-NiO and Al_2O_3-Cr_2O_3, or in an extensive composition range in the neighborhood of intermediate phases, e.g., $3Al2O_3 \cdot 2SiO_2$ (mullite s.s.) in the SiO_2-Al_2O_3 system.

3.1.1 The solid solution in the combeite structure

Maki and Sugimura first recognized a continuous solid solution of combeite $Na_{4+2x}Ca_{4-x}[Si_6O_{18}]$ ($0 < x < 1$) in the $Na_2O \cdot 2CaO \cdot 3SiO_2$-$Na_2O \cdot CaO \cdot 2SiO_2$ pseudo-binary system [29]. Later, these authors reported that the division of M2 sites in the high-temperature structure

creates vacancies in M22 sites of the low-temperature form which accommodates additional cations in the structure [40,41]. Thus, the precipitation of combeite s.s. is due to the exchange of Ca^{2+} by two Na^{+} ions, with extra Na^{+} occupying M22 sites.

One of the main effects of the composition change is readily observed by differential thermal analysis (Figure 9). The stoichiometric combeite presents a hexagonal to rhombohedral polymorphic transformation at T_{pm} = 485 °C, by increasing the Na_2O content in the parent glass, the T_{pm} shifts to lower temperatures [29]. Fokin and Zanotto reported the same behavior during crystallization of glasses in the $Na_2O{\cdot}SiO_2$ -$CaO{\cdot}SiO_2$ pseudo-binary join [3]. Macena also observed the deviation of T_{pm} in the pseudo-binary system studied in this work.

Figure 9: Differential thermal analysis curves of glasses in the $Na_2O{\cdot}2CaO{\cdot}3SiO_2$-$Na_2O{\cdot}CaO{\cdot}2SiO_2$ pseudo-binary.

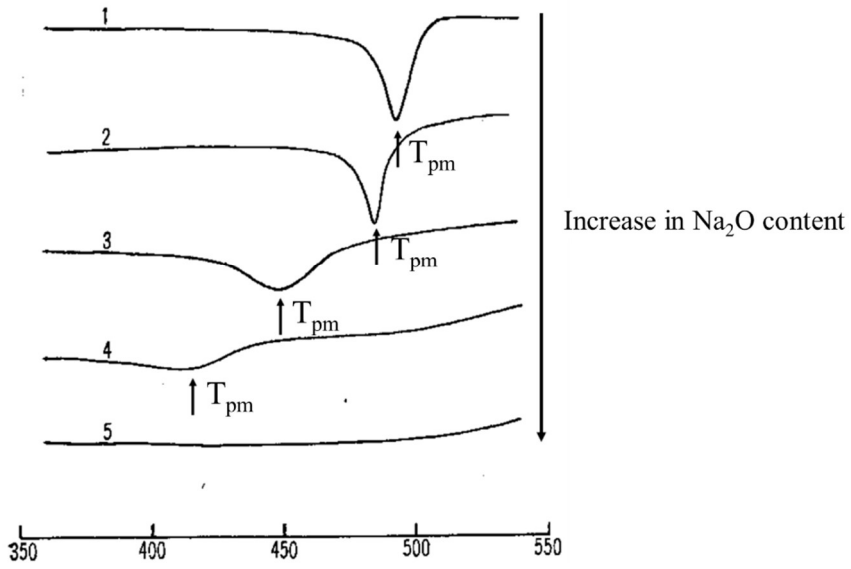

Source: Adapted from Maki and Sugimura (1968) [29]

On the effect of combeite s.s. in the crystallization kinetics of soda-lime-silicate glasses, Fokin *et al.* concluded that the growth of this phase led to a change in the glass matrix composition accompanied by the formation of a diffusion zone in the crystal vicinity [43]. When samples containing pre-existing crystals were heat-treated at low temperatures (T = 1.01Tg), the nucleation in the neighborhood of Na^{+}-rich crystals was hindered by the reduced concentration of Na^{+} in the residual glass. The decrease in Na^{+} content is associated with the increase of crystal-liquid interface energy, which, in turn, is inversely related to the thermodynamic barrier for crystallization [44].

In other works, the composition shift from stoichiometry was also observed in crystals formed in stoichiometric and nonstoichiometric glasses [3,4]. Since the composition of the nucleated phase may be different from the precursor glass, even stoichiometric ones, one may raise the hypothesis of a misconception in the CNT due to the assumption that stoichiometric nuclei present the same properties of the final macro-phase.

Macena observed that combeite is the only phase to crystallize in the volume of glasses in the C-D system; however, further investigations were necessary [6]. Also, it was reported in the same work, the presence of unknown phases of compositions close to the eutectic.

4 GOALS

Motivated by what was presented above, the goals of this work are:

- Investigate the formation of combeite solid solution in compositions between 0 and 33.3 mol% devitrite belonging to the $Na_2O{\cdot}2CaO{\cdot}3SiO_2$-$Na_2O{\cdot}3CaO{\cdot}6SiO_2$ pseudo-binary join by analyzing the lattice parameters of combeite crystallized.
- Characterize the crystallized phases in glasses with 33.3 and 50 mol% devitrite.

5 MATERIALS AND EXPERIMENTAL TECHNIQUE

5.1 Glass Preparation

The compositions were defined to complement the study on the crystallization kinetics of non-stoichiometric glasses in the combeite-devitrite system initiated in the Vitreous Materials Engineering Group (GEMaV) of the Department of Materials Engineering at the São Carlos School of Engineering, University of São Paulo [6]. The studied glass compositions begin at the stoichiometric combeite and extend to devitrite, these end components are represented by the ratios 1:2:3 and 1:3:6, respectively, as shown in Figure 4.

Glasses were synthesized from the analytical grade reactants: quartz (99.9%, Zetasil 3 Santa Rosa, Brazil), anhydrous Na_2CO_3 (99.5%, *Labsynth*, Brazil) and $CaCO_3$ (99%, *Labsynth*, Brazil). The raw materials were previously dried at 120 °C for 2 h in a laboratory oven (*Venticell*, 111 L, *MMM Group*, German) and weighed in an analytical balance (AUX220, *Shimadzu,* Japão) according to Table 1. Then, for better homogeneity, the 150 g batches were mixed in an alumina ball mill for 3 h.

Table 1: Nominal batch compositions together with compositions investigated by Macena (2019) indicated with an *

Glass	The proportion of the end components of the binary joint		The proportion of the oxide components of the Na_2O-CaO-SiO_2 system		
	Combeite (%mol)	Devitrite (%mol)	Na_2O (%mol)	CaO (%mol)	SiO_2 (%mol)
C *	100	0	16.67	33.33	50
$C_{15}D$	93.75	6.25	16	33	51
C_7D *	87.5	12.5	15.38	32.69	51.43
C_3D *	75	25	14.29	32.14	53.57
C_2D *	66.7	33.33	13.64	31.82	54.54
C_7D_5	58.33	41.67	13.04	31.52	55.43
CD *	50	50	12.5	31.25	56.25
C_3D_5	37.5	62.5	11.76	30.88	57.35
CD_3 *	25	75	11.11	30.56	58.33
C_3D_{13}	18.75	81.25	10.81	30.40	58.78

CD_{15}	6.25	93.75	10.26	30.13	59.61
D *	0	100	10	30	60

Source: Author (2021)

A bottom-load electric furnace (DT-31-RS-78-E3504, *Deltech Inc*., EUA) was used to melt the batches in a platinum crucible between 1350 to 1400 °C (Table 2). The glasses were manually stirred every 15 min for the first 2 h of melting to ensure homogeneity. After approximately 5 h, the molten compositions were poured and pressed between two stainless steel plates (splat cooling) to freeze below T_g, into glassy samples, which then were let to cool down to room temperature.

Table 2: Glass samples synthesis temperatures.

Glass	Synthesis temperature (°C)
C	1350
$C_{15}D$	1350
C_7D_5	1400
C_3D_5	1400
C_3D_{13}	1400
CD_{15}	1400

Source: Author (2021)

5.2 Differential Scanning Calorimetry (DSC) – Characteristic Temperatures

DSC is a thermal analysis technique that measures the heat flowing into or out of a sample as a function of temperature. The resulting curve indicates the material's physical and chemical transformations as endothermic or exothermic peaks and baseline shifts.

Each glass had its characteristic temperatures, namely, crystallization temperature, T_x, polymorphic transition temperature, T_{pm}, *solidus* temperature, T_S, *liquidus* temperature, T_L, and glass transition temperature, T_g, characterized by a DSC 404 F1 Pegasus, NETZSCH. Glass monoliths samples weighing approximately 10 mg were used as samples in a platinum crucible and analyzed on heating and cooling at 10 K/min, using synthetic air as atmosphere. Table 3 shows the samples' masses and their temperature range of analysis.

Table 3: Samples' mass subjected to DSC and corresponding temperature range of measurement.

Composition	Sample mass (mg)	Temperature range (°C)
C	10.8	300 – 1400
$C_{15}D$	10.8	300 – 1400
$C_{10}D$	11.0	300 – 1400
C_2D	11.5	300 – 1400
C_7D_5	11.1	300 – 1400
CD	10.9	300 – 1400
C_3D_5	11.2	300 – 1400
C_3D_{13}	10.6	300 – 1400
CD_{15}	11.8	300 – 1400

Source: Author (2021)

5.3 Differential Scanning Calorimetry (DSC) – Non-isothermal treatments

DSC was also used to study the behavior of phase transformation at non-isothermal treatments.

Monoliths and powdered samples of C_2D and CD compositions weighing ~10 mg were analyzed on heating/cooling at 5 °C/min until 1400 °C. A lower heating/cooling rate was adopted to increase the resolution in determining the temperature range in which the reactions occur. The difference in the behaviors presented by the monolith and powdered samples allows one to assess the crystallization behavior, such as whether different reactions overlap or the effect of surface crystallization. Platinum crucibles and synthetic air were used in the DSC runs.

Table 4: DSC heat treatment parameters for composition C_2D and CD. The heating/cooling rates were 5 °C/min.

Composition	Sample	Sample mass (mg)	Temperature range (°C)
C_2D	Powder	11.5	300 – 1400
	Bulk	10.7	300 – 1400
CD	Powder	11.2	300 – 1400
	Bulk	10.9	300 – 1400

Source: Author (2021)

Two crystallization peaks were identified in the DSC curves of samples indicated in Table 4, except for the bulk C_2D sample, which presented only one peak. The crystallization

peaks temperatures were used to design non-isothermal treatments in a DSC (Figure 10 and Figure 11). Powder and bulk samples were then subjected to the following heat-treatments and posteriorly used to study the phases formed in each peak by XRD:

Set 1. i) Heating from room temperature to 300 °C at 20 °C/min; ii) dwell time of 15 min to stabilize the temperature; iii) heating to the first crystallization peak at 5 °C/min; iv) dwell time of 15 min; v) cooling down to room temperature at 5 °C/min.

Set 2. i) Heating from room temperature to 300 °C at 20 °C/min; ii) dwell time of 15 min to stabilize the temperature; iii) heating to the first crystallization peak at 5 °C/min; iv) dwell time of 15 min; v) cooling down to 300 °C at 5 °C/min; vi) dwell time of 15 min to stabilize the temperature; vii) heating to the second crystallization peak at 5 °C/min; viii) heat treating at the second crystallization peak temperature for 15 min; and ix) cooling down to room temperature at 5 °C/min.

Powder and bulk samples of ~85 mg were crystallized in the DSC in a platinum crucible and synthetic air. Figure 10 and Figure 11 summarize the treatments. The bulk C_2D sample did not present two crystallization peaks. Therefore, only powdered C_2D glass was subjected to the treatment sets.

Figure 10: DSC heat-treatments for composition CD.

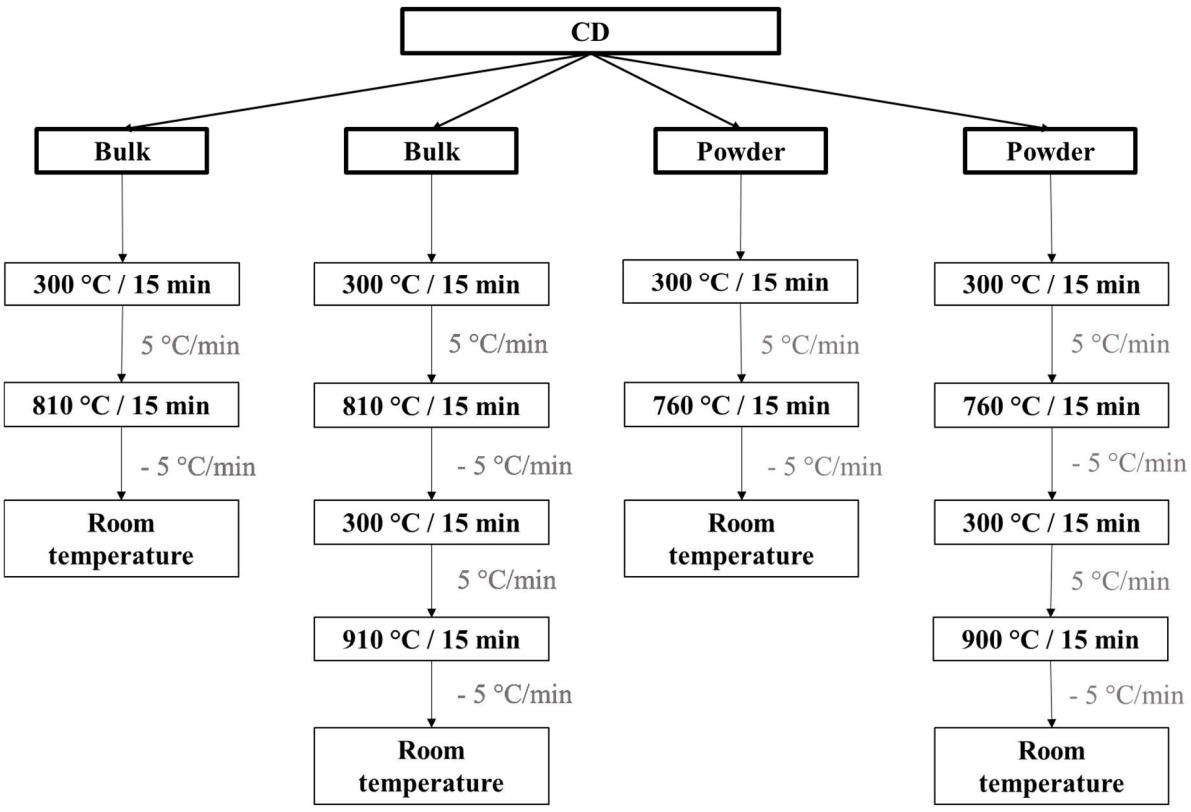

Source: Author (2021)

Figure 11: DSC heat-treatments for composition C_2D.

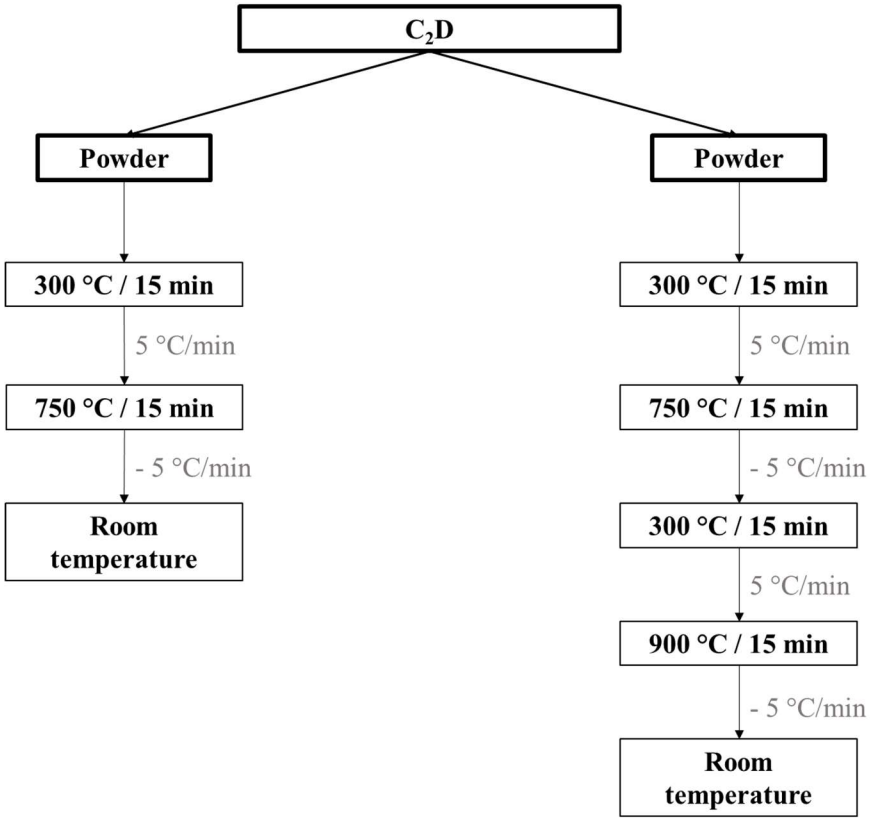

Source: Author (2021)

After the non-isothermal treatments, the samples were grounded under 50 μm and analyzed by XRD (Rotaflex equipment, RU200B, Rigaku, Japan), with CuK$_\alpha$ radiation (λ_w= 1,54 Å) at 40 kV and 60 mA to identify the phases crystallized in each exothermic DSC peak. The analyses took 90 min for 2θ from 10 ° to 70 °.

5.4 Phase characterization of glass C_2D and CD

The C_2D glass was cut into cubic samples of 2 mm edge length and isothermally treated at 730 °C, close to the onset of the first crystallization peak, for different times as summarized in Figure 12: Times of the isothermal treatments of C_2D cubic samplesFigure 12.

Figure 12: Times of the isothermal treatments of C_2D cubic samples (2 mm edge length) at 730 °C.

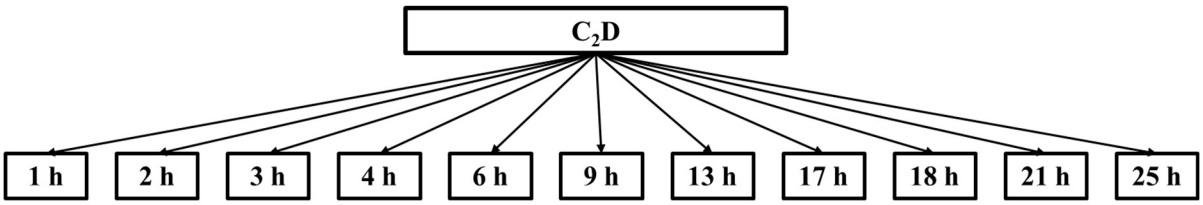

Source: Author (2021)

Samples treated at 9 h and 21 h were grounded and subjected to XRD: 10° < 2θ < 70 °, step 0.0200° /s, and CuKα radiation (λ_w= 1,54 Å) at 40 kV and 60 mA to determine the crystallized phases in the surface layer and the bulk of the heat-treated glass. Then, the samples were non-isothermally treated during DSC runs in platinum crucibles and synthetic air heating from 300 °C to 1000 °C and cooling down to room temperature at 10 °C/min.

T_g and T_{pm} on heating were measured from the DSC curves. The glass transition temperature provided an estimation of the residual glass composition for glasses that crystallized two phases in the equilibrium. As the primary phase crystallizes, the T_g of the residual glass approaches the T_g of the glass which chemical composition is equivalent to the second crystalline phase. In this work, it was expected that all compositions, except C and D, crystallize combeite and devitrite in different proportions in the equilibrium.

To verify the peritectic reaction of devitrite at temperatures above 1030 °C, cubic C_2D samples (2 mm edge length) previously heat-heated at 730 °C for 4 and 25 h were non-isothermally treated up to 1250 °C at 10 °C/min. The treatments were carried out in a DSC using platinum crucible and synthetic air. The presence of this transformation confirms whether devitrite had crystallized after the non-isothermal treatments.

Also, samples of CD glass were cut into cubic samples with an edge of 2 mm, which were isothermally treated at 775 °C for 90, 120, 150 and 240 min. This temperature is approximately the crystallization onset of this glass. Optical microscopy (DM4P, Leica, Germany) was performed in samples ground and polished with cerium oxide and etched with a mixture of hydrofluoric and hydrochloric acids during 20 s. Energy dispersive spectroscopy, EDS, dot map (FEI, Inspect F50, USA) was used to verify the presence of diffusion zones in the sample treated at 120 min. Also, the phase formation of the fully crystallized sample (240 min) was analyzed by XRD: 10° < 2θ < 70 °, step 0.0200 /s, and CuKα radiation (λ_w= 1,54 Å) at 40 kV and 60 mA.

The microstructure of the crystallized phases in both C_2D and CD compositions were studied by reflected light optical micrography (DM4P, Leica, Germany).

5.5 Crystallization above solidus, T_S

To study the phase transformations at temperatures above T_S, C_2D and CD compositions were melted at 1350 °C and held at this temperature for 20 min. Then, the samples were cooled down to 1100 °C at -10 °C/min and let at this temperature for 20 and 90 min, respectively. After the treatments, they were immediately cooled down to room temperature by removing them from the furnace. Finally, the microstructures and chemical composition were analyzed by optical microscopy and scanning electron microscopy, MEV, (FEI, Inspect F50, USA) and EDS (FEI, Inspect F50, USA).

Also, D glass was grounded and heat-treated at 1100 °C for 72 h to induce surface crystallization. The crystalline phases were determined by XRD, $10° < 2\theta < 70$ °, step 0.0200 /s, and CuKα radiation (λ_w= 1,54 Å) at 40 kV and 60 mA.

5.6 Heat treatments for lattice parameter measurement

Heat treatments were performed in a vertical electric furnace with ZAS (zirconia-alumina-silica) crucible as a sample holder and a K-type thermocouple with temperature control within 1 °C. Except for combeite and devitrite glasses, the glass samples were subjected to two-isothermal treatments for nucleation and crystal growth, a procedure known as the Tammann or development method (Table 5) [45,46]. As discussed in section 2.2, crystal nucleation and growth rates reach a maximum at some temperature. Despite the overlapping of these curves, one can determine a range of temperatures at which the nucleation rate is high, and the crystal growth rate is insignificant, or the reverse. In the development method, the heat treatment is first stepped at a temperature for nucleation, T_n, and then driven up to a temperature for crystal growth or development, T_d, with $T_n < T_d$. This procedure is helpful to study nucleation kinetics since the size of critical nuclei is undetectable by most experimental techniques. The heat treating at T_d makes the nuclei grow as observable crystals by optical or electronic microscopy.

Due to de drastic decrease in I_{st} with the increase in SiO_2 content, only glasses with a composition containing less than 33.3 mol% of devitrite showed homogeneous nucleation.

Table 5: Heat treatment parameters used for lattice parameter study.

Glass	Form of sample	Heat treatment (°C)
C	Bulk	700 °C/3 days
$C_{15}D$	Bulk	590 °C/30min + 720 °C/18min
C_7D	Bulk	600 °C / 37 min + 720 °C / 28 min
C_3D	Bulk	600°C / 3h + 720 °C / 1h55min
C_2D	Bulk	582 °C / 5days + 740 °C / 46min
D	Powder	1100°C / 3 days

Source: Author (2020)

The heat-treatments were projected to produce 20000 nuclei/mm^3 and to obtain samples 100 % crystallized. The nucleation, I_{st}, and crystal growth, U, rates of C, C_3D and, C_2D glasses are known from the literature [7]. For $C_{15}D$ and C_7D, the nucleation and development temperatures were chosen between the T_g and T_x and based on the data of C, C_3D and, C_2D glasses. Glasses C and D were treated at relatively high temperatures, which makes the development method unnecessary. The former presented rapid volume crystallization; therefore, the development method was not necessary. Before being analyzed by optical microscopy, the heat-treated samples were embedded in epoxy resin, ground, polished with cerium oxide, and etched with a mixture of hydrofluoric and hydrochloric acids during 20 s.

5.7 X-Ray Diffraction (XRD) – Combeite solid solution investigation

According to section 3.1.1, combeite can crystallize as solid solutions. The precipitation of Cs.s. was described as the nucleation of a Na-enriched crystal at early crystallization stages. The substitution of one Ca^{2+} by two Na^+ causes the reduction of the thermodynamical barrier to nucleation by decreasing the crystal-liquid surface energy. As the crystal growth proceeds, the composition of the crystals approaches stoichiometry due to the reduction of Na cations in the residual glass. In the literature, the formation of Cs.s. was accompanied by an increase in the *a* parameter of the hexagonal crystalline structure with the increase in Na_2O content [4,39]. Thus, by measuring the variation of lattice parameters as a function of composition, one can estimate the compositional range in which the Cs.s. occurs.

The characterization of the combeite lattice parameters was performed by XRD (Rotaflex equipment, RU200B, Rigaku, Japan), $10° < 2\theta < 70$ °, using step scan mode, step 0.0200 /s, 5 s/step, and CuKα radiation (λ_w= 1,54 Å) at 40 kV and 60 mA. The database of

ICDD (International Center for Diffraction Data) was used to identify the diffraction planes and the present phases.

In equilibrium at room temperature, the combeite has a hexagonal crystalline structure. Therefore, the lattice parameters a and c are given by Eq. (8):

$$\frac{1}{d^2} = \frac{4}{3}\left(\frac{h^2 + hk + k^2}{a^2}\right) + \frac{l^2}{c^2} \quad ((8)$$

where *hkl* are the indices of the diffraction planes, and d is the distance between diffracting crystalline planes given by Eq. (9).

$$n.\lambda_w = 2d.\sin\theta \quad (9)$$

where, n is the order of the reflection and λ_w the wavelength of incident X rays.

The glasses heat-treated as shown in Table 5 were used to study the solid solution formation between 0 and 33.3 mol % of D. After the treatments, the samples were ground into a powder (< 50 μm) and blended with powdered silicon. The Si diffraction pattern (ICDD 00-027-1402) was used as a reference. The most intense peak of the Si diffractogram was chosen for the corrections of the combeite peaks, which corresponds to the plane (111) at 2θ = 28,443 °. Three samples of each composition were subjected to XRD for statistical purposes ANOVA analysis was performed with a 95% confidence interval.

A partially crystallized sample of C_2D glass was analyzed by SEM with backscattered electron, BSE, and EDS to investigate compositional gradients.

6 Results and discussion

6.1 Characteristic temperatures

Figure 13 shows the DSC curves of the compositions studied in this work. Figure 14 shows a zoomed view of the DSC curves of C_2D on heating (a) and cooling (b).

Figure 13: DSCs of studied compositions using bulk samples without previous heat treatments (10 °C/min): on (a) heating and (b) cooling.

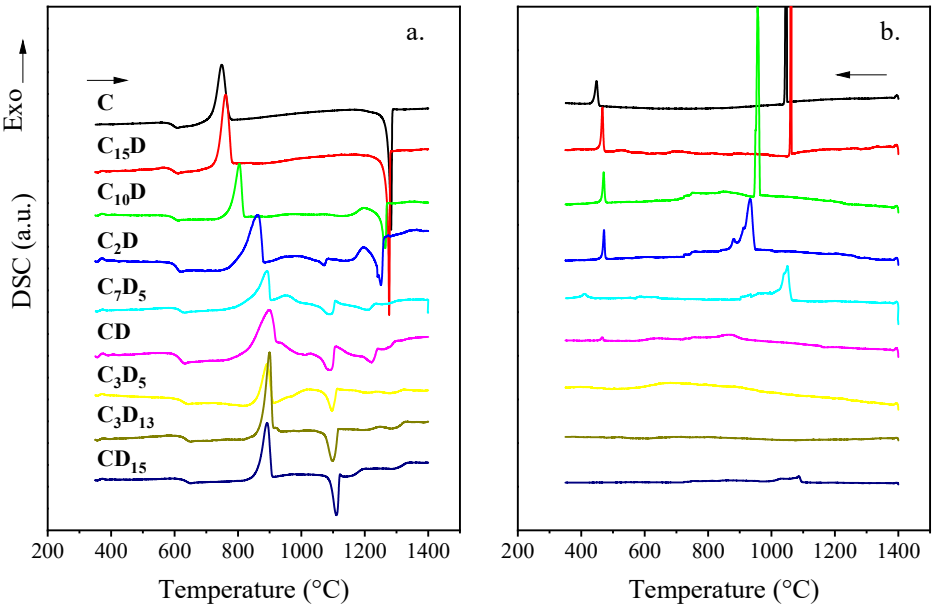

Source: Author (2021)

Figure 14: Typical DSC heating (a.) and cooling (b.) curves performed at 10 °C/min. Zoomed view of C_2D glass taken from Figure 13.

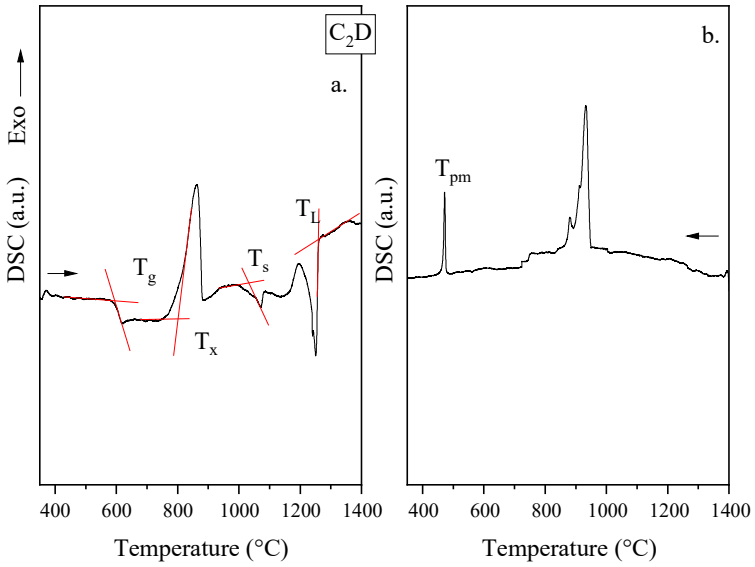

Source: Author (2021)

Figure 15: Characteristic temperatures according to DSC curves as a function of molar fraction of devitrite.

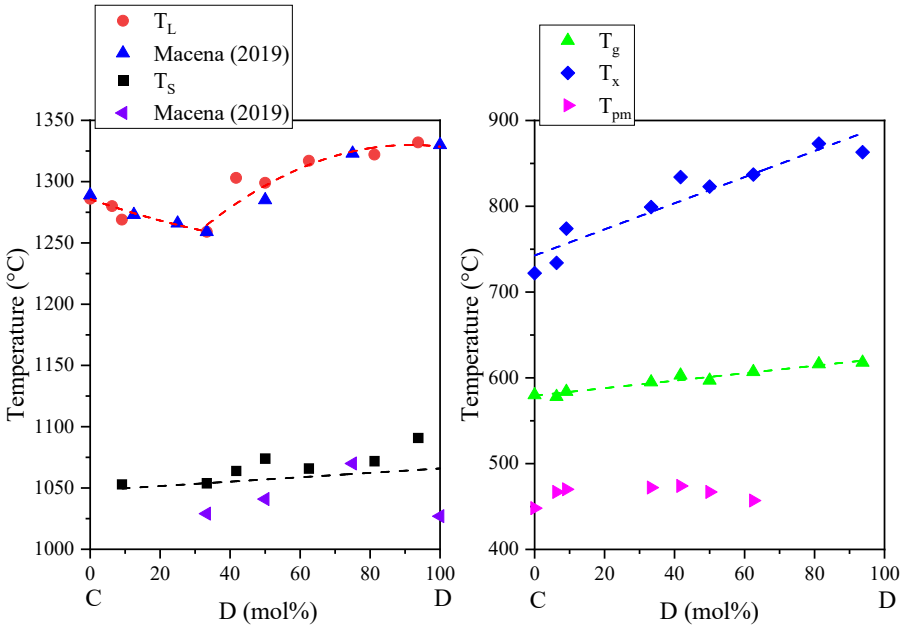

Source: Author (2021)

The characteristics temperatures of the compositions are summarized in Table 6.

Table 6: Characteristic temperatures according to DSC curves of bulk samples (10 °C/min). T_g, T_x, T_S and T_L were measured during heating and T_{pm} during cooling.

Composition	T_g (°C)	T_x (°C)	T_S (°C)	T_L (°C)	T_{pm} (°C)
C	580	722		1286	448
$C_{15}D$	578	734		1280	467
$C_{10}D$	584	774	1053	1269	470
C_2D	595	799	1054	1259	472
C_7D_5	603	834	1064	1303	474
CD	597	823	1074	1299	467
C_3D_5	607	837	1066	1317	457
C_3D_{13}	616	873	1072	1322	--
CD_{15}	618	863	1091	1332	--

Source: Author (2021)

Figure 15 shows the dependence of T_g, T_x, T_s, T_L, and T_{pm} on the composition. T_g and T_x monotonically increased by increasing devitrite content, probably due to the increase in the supercooled liquid viscosity. The temperatures corroborate and complete previous data published by [6].

According to Figure 13, glasses with more than 33.3 mol% D present more complex behavior on their heating path. For C_2D glass, an endothermic peak can be identified at 1054

°C, increasing in intensity and shifting towards higher temperatures as D content increases. Also, DSC curves of C_7D_5 and CD glasses presented two crystallization peaks.

Figure 16: Crystallization path of C_2D and CD compositions from T_L until complete crystallization in equilibrium.

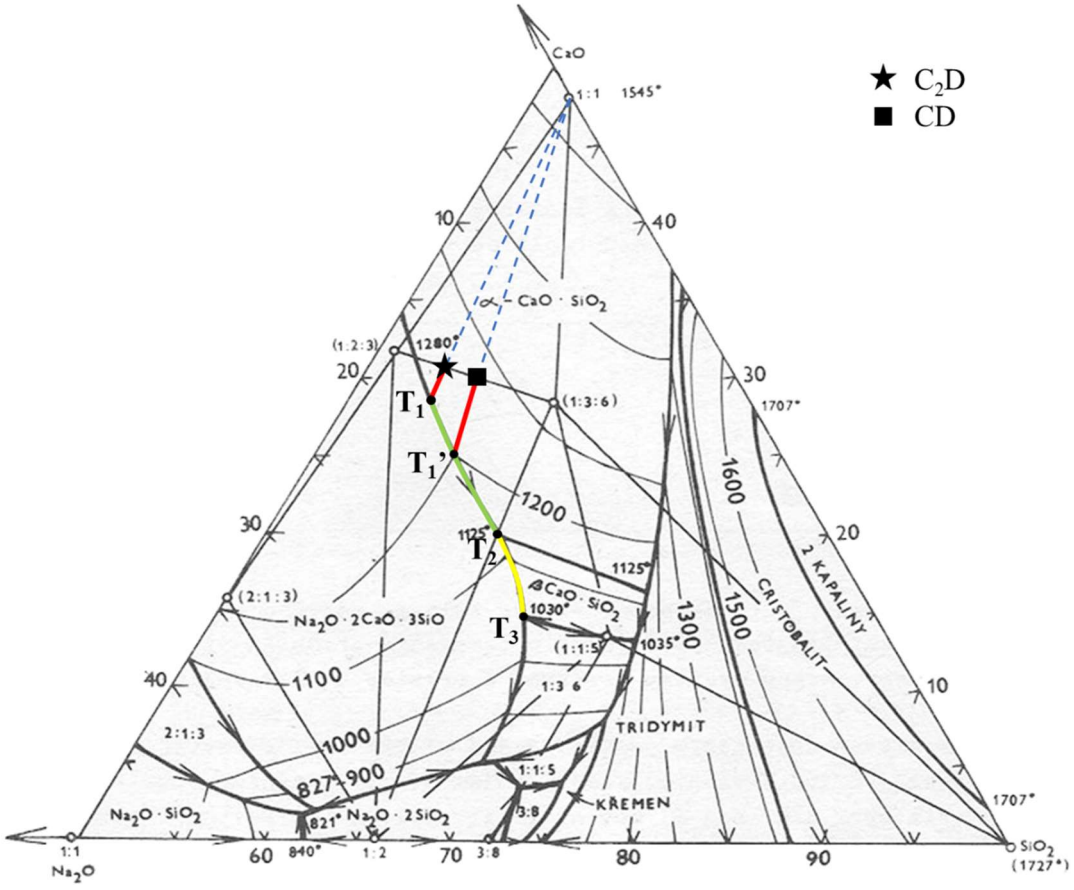

Source: Adapted from Shadid and Glasser (1972) [28]

Figure 16 shows an equilibrium phase diagram of Na_2O – CaO – SiO_2. On cooling from the T_L to T_1 or T_1', respective to C_2D and CD compositions, the crystallization begins by forming primary α-wollastonite crystals, leading to a residual glass richer in Na^+. Below T_1 or T_1', the crystallization of combeite takes place. At T_2 = 1125 °C, α-wollastonite changes from the high-temperature to low-temperature form, β-wollastonite, releasing latent heat. As glass cooling proceeds, β-wollastonite and the residual liquid transform into devitrite below T_3 = 1030 °C (peritectic reaction). The cooling path refers to compositions between 11.9 and 93.7 wt % D. The C – D pseudo-binary phase diagram is given in Figure 17 according to the equilibrium ternary diagram.

Figure 17: Phase diagram of the C-D pseudo-binary join.

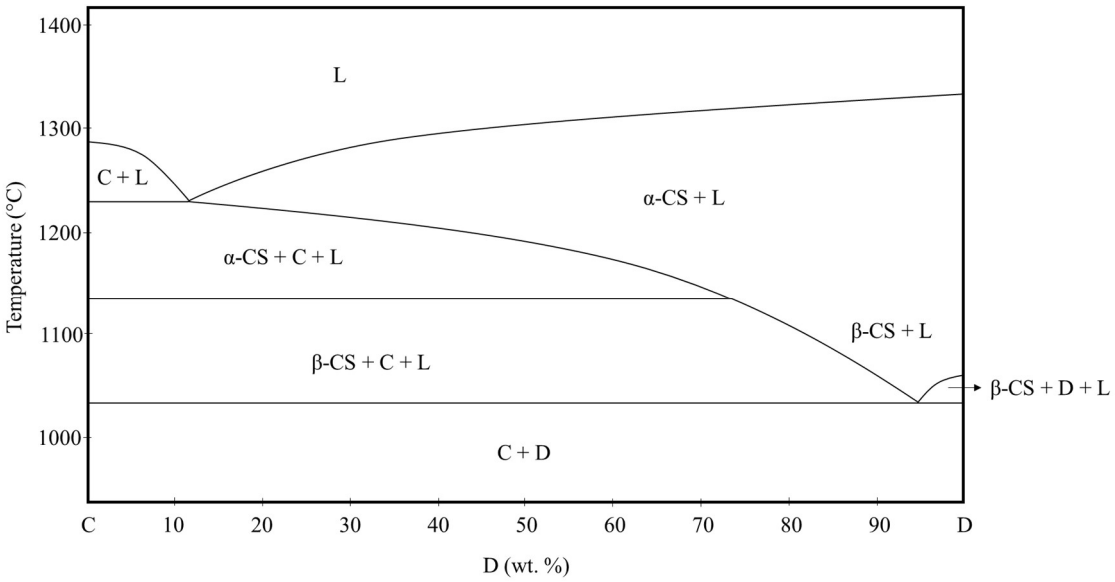

Source: Adapted from Shadid and Glasser (1972) [28]

According to the phase diagram of Figure 17, except for the end compositions, all other compositions between C and D are expected to crystallize below 1030 °C completely. However, glassy materials are not in thermodynamic equilibrium. Therefore, the resultant phases after some heat treatment might differ from expected in the above-illustrated phase diagrams. Also, crystallized phases on heating and cooling paths can be different, as glasses undergo non-equilibrium transformations (relaxation and, eventually, crystallization).

6.2 Phase characterization of compositions CD and C_2D.

DSC curves of powder and monolithic samples of the CD and C_2D compositions are shown in Figure 18 and Figure 19, respectively. A rate of 5 °C/min, lower than the one used in the DSC runs presented in Figure 13, was used to analyze the surface effect on the crystallization peaks. CD glass showed two exothermic peaks on the heating of both powder and bulk samples (Figure 18). A second exothermic peak also appeared in the DSC curve on heating the C_2D glass composition, the closest to the higher-temperature eutectic in the C -D system among the studied compositions [6].

In both compositions, CD and C_2D, the crystallization peaks of powder samples shifted to lower temperatures than monolithic ones, related to the higher tendency of glass powders to crystallize from heterogeneous nucleation sites on the surface of the particles [47].

Figure 18: DSC curves performed at 5 °C/min of bulk and powdered samples of CD composition a) heating up to 1400 °C and b) cooling down to the room temperature.

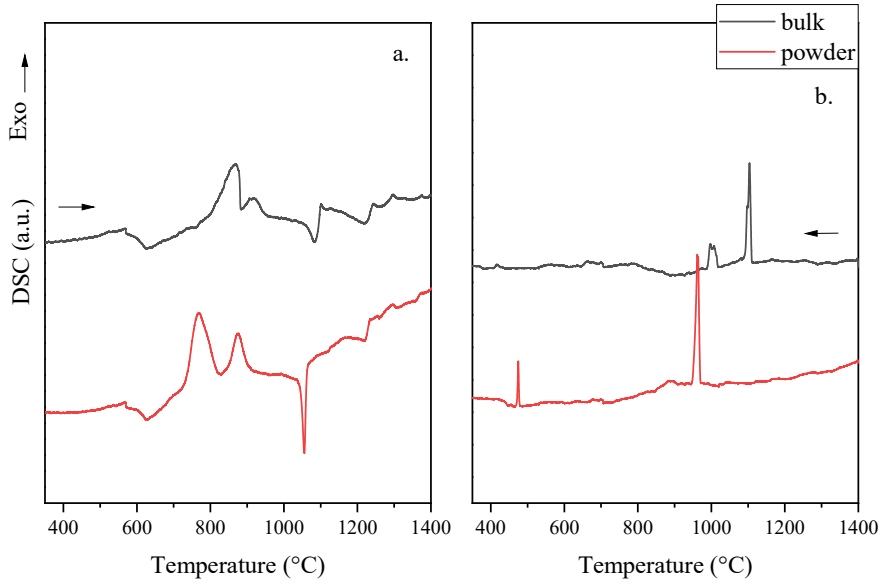

Source: Author (2021)

Figure 19: DSC curves performed at 5°C/min of bulk and powdered samples of C_2D composition a) heating up to 1400 °C and b) cooling down to room temperature.

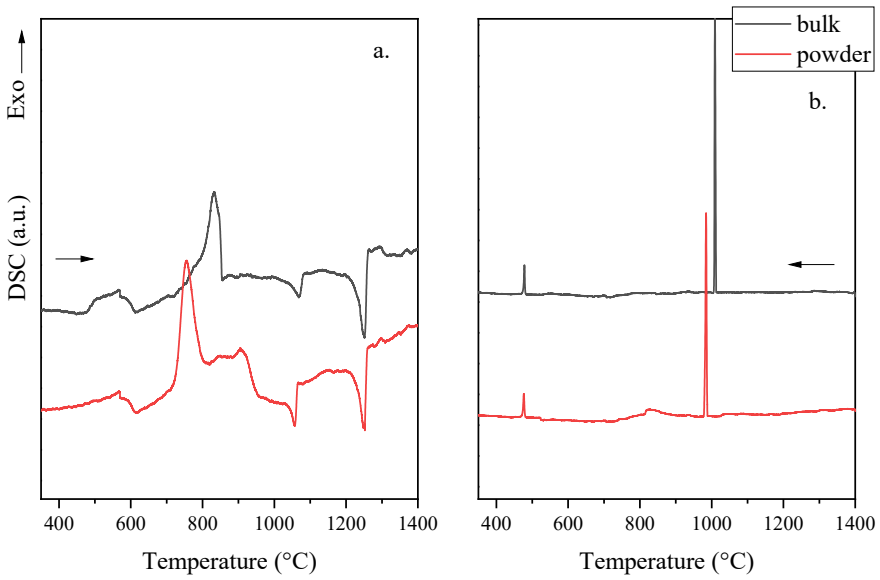

Source: Author (2021)

As described in section 5.3, non-isothermal treatments of powder and bulk samples were performed based on previous DSC runs to investigate the phases formed in the first and second

crystallization peaks. The treatments temperatures were settled based on the DSC curves observed in Figure 18 and Figure 19.

Figure 20, Figure 22 and Figure 24 show the DSC curves of samples heated from 300 °C up to the first crystallization peak, cooled down to 300 °C, heated up to the second crystallization peak and cooled down to the room temperature. Figure 21, Figure 23 and Figure 25 show the XRD results of samples after these treatments.

Figure 20: DSC runs (5 °C/min) of powdered C_2D glass subjected to non-isothermal treatments 1) heated up to 750 °C and treated at 750 °C for 15 min, 2) cooled down to 300 ° C (dwell time of 15 min to stabilize the temperature), 3) heated up to 900 °C and treated at 900 °C for 15 min and, 4) cooled down to room temperature.

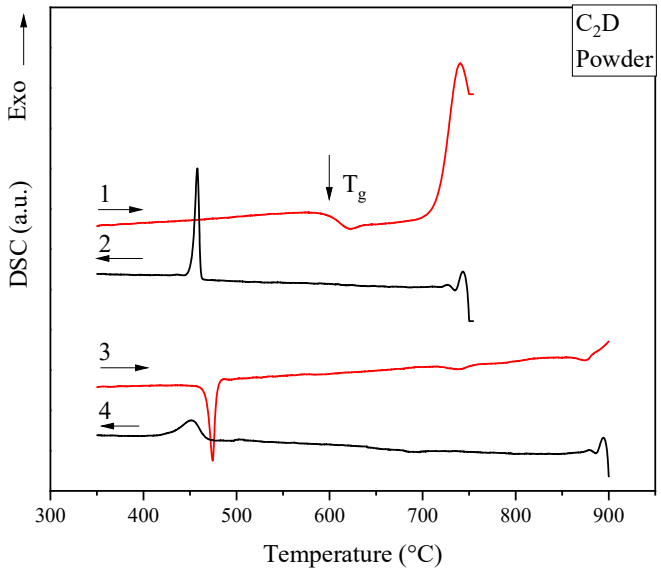

Source: Author (2021)

Figure 21: Diffractograms of powdered C_2D glass subjected to non-isothermal treatments a) heated up to 750 °C and treated at 750 °C for 15 min; and b) heated up to 750 °C and treated at 750 °C for 15 min

cooled down to 300 ° C (dwell time of 15 min to stabilize the temperature) + heated up to 900 °C and treated at 900 °C for 15 min + cooled down to room temperature.

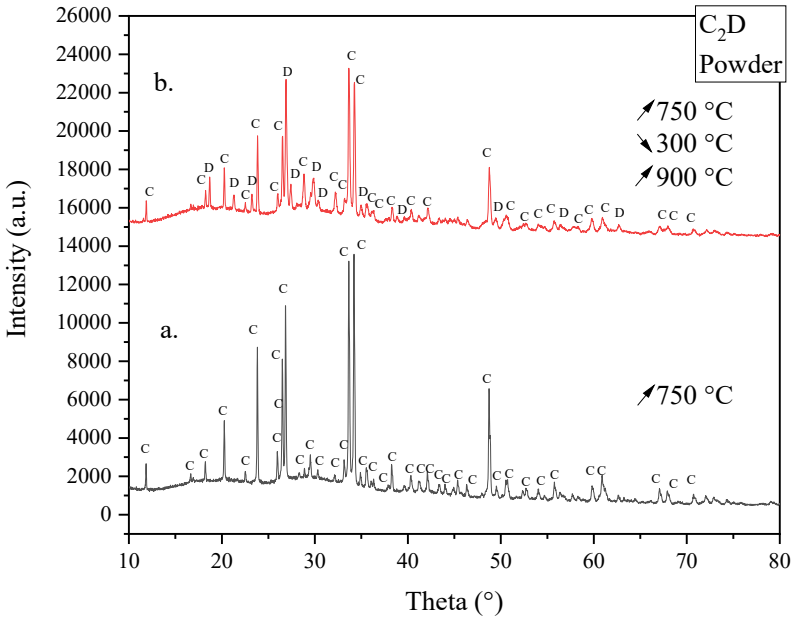

Source: Author (2021)

Figure 22: DSC runs (5 °C/min) of powdered CD glass subjected to non-isothermal treatments 1) heated up to 760 °C and treated at 760 °C for 15 min; 2) cooled down to 300 °C (dwell time of 15 min to stabilize the temperature); 3) heated up to 900 °C and treated at 900 °C for 15 min; and, 4) cooled down to room temperature.

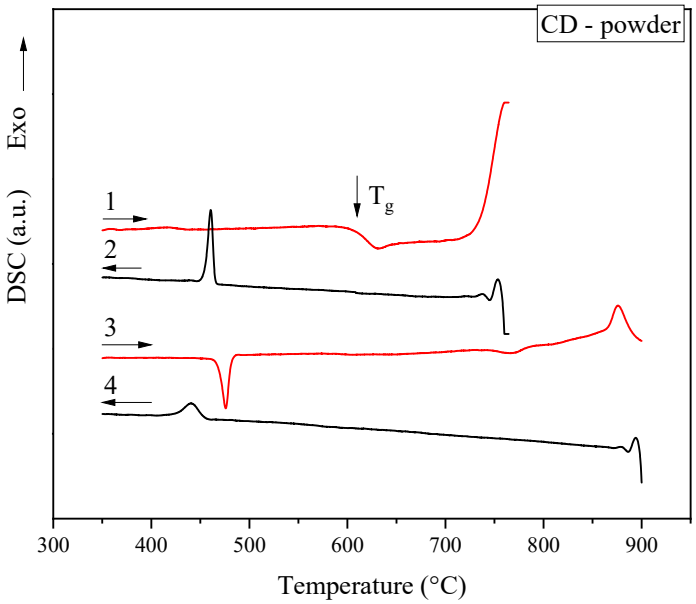

Source: Author (2021)

Figure 23: Diffractograms of powdered CD glass subjected to non-isothermal treatments a) heated up to 760 °C and treated at 760 °C for 15 min; and b) heated up to 760 °C and treated at 760 °C for 15 min + cooled down to 300 ° C (dwell time of 15 min to stabilize the temperature) + heated up to 900 °C and treated at 900 °C for 15 min + cooled down to room temperature.

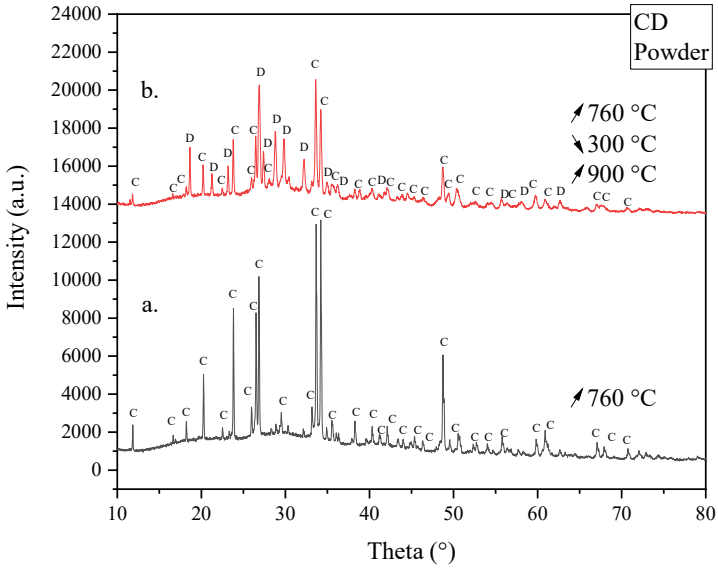

Source: Author (2021)

Figure 24: DSC runs (5 °C/min) of powdered CD glass subjected to non-isothermal treatments 1) heated up to 810 °C and treated at 810 °C for 15 min; 2) cooled down to 300 °C (dwell time of 15 min to stabilize the temperature); 3) heated up to 910 °C and treated at 910 °C for 15 min; and, 4) cooled down to room temperature.

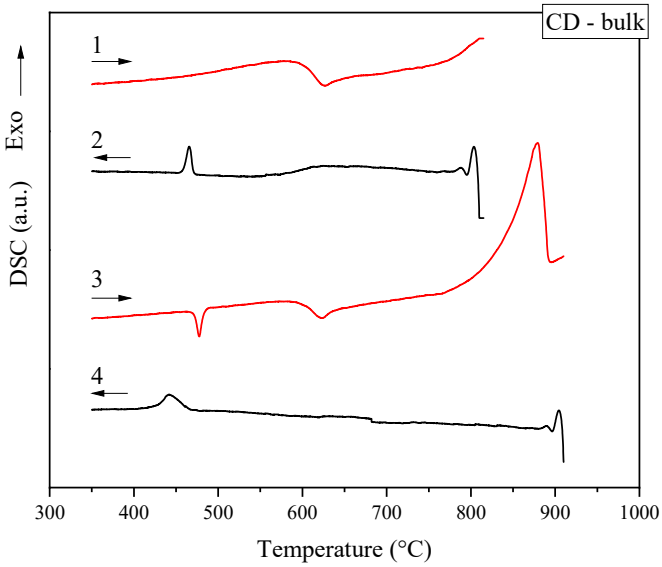

Source: Author (2021)

Figure 25: Diffractograms of bulk CD glass subjected to non-isothermal treatments a) heated up to 810 °C and treated at 810 °C for 15 min; and b) heated up to 810 °C and treated at 810 °C for 15 min + cooled down to 300 ° C (dwell time of 15 min to stabilize the temperature) + heated up to 910 °C and treated at 910 °C for 15 min + cooled down to room temperature.

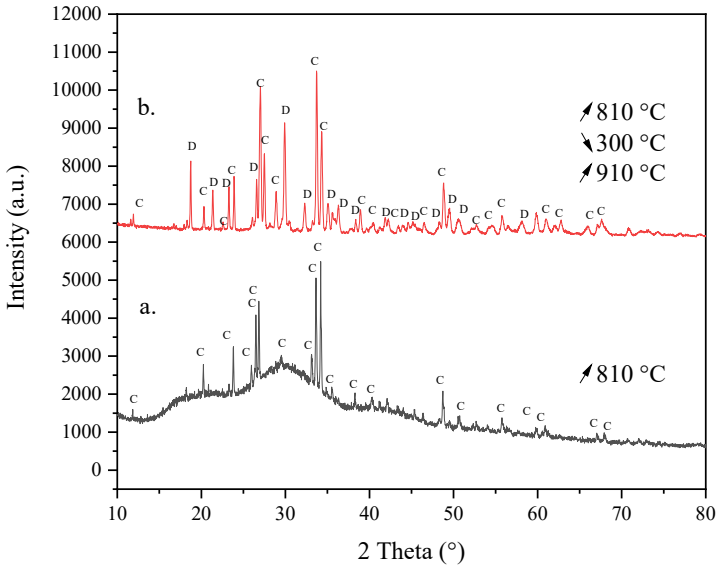

Source: Author (2021)

According to Figure 21, Figure 23, and Figure 25, both glasses C_2D and CD, regardless of the sample form (bulk or powder), showed combeite (ICDD 01-079-1089) as the crystallized phase in the first exothermic peak. Furthermore, the diffractograms also indicated the presence of combeite and devitrite (ICDD 00-023-0671) after double-stage treatment at first and second exothermic peaks. Nevertheless, all XRD presented a background corresponding to residual glass.

The crystallization of combeite on the heating to the first crystallization peak was confirmed by its polymorphic transition peak at temperatures approximately 460 °C on the subsequent cooling. (Table 7).

Table 7: Polymorphic transition temperature and peak area of the combeite polymorphic transition, A_{pm}, during non-isothermal treatments.

	T_{pm} (°C)			A_{pm} (a.u.)	
Glass	**1º cooling**	**2 ° heating**	**2º cooling**	**1º cooling**	**2º cooling**
C_2D_{powder}	458	474	451	0,80602	0,53959
CD_{powder}	461	475	440	0,69979	0,34547
CD_{bulk}	465	477	441	0,17603	0,30974

Source: Author (2021)

After heat-treatment to the second exothermic peak, the combeite polymorphic transition peaks changed on the subsequent cooling and shifted to lower temperatures. It is known that changing the composition of the crystals substantially affects the polymorphic transition temperature. In the present case, the increase in sodium concentration in combeite crystals shifts their polymorphic transformation to lower temperatures (Figure 9)[3,4,29]. Additionally, the peak widening is also related to composition variation. Narrow peaks mean the crystals' compositions are very close to each other. Thus, they undergo phase transformation more simultaneously. In cases that the average deviation of the sample composition is significant, i.e., there is a large distribution of crystals with different compositions, the peak becomes broad. Therefore, the combeite crystals at the end of the second treatment in Figure 20, Figure 22, and Figure 24 have higher average sodium concentrations than those formed during the first heating and a wide compositional gradient. This compositional deviation was markedly high for CD glass (12.5 mol% Na_2O) since T_{pm} varied up to 19 °C.

The crystallized volume fraction of combeite after a heating treatment can be assessed through the area of the polymorphic transition peak, A_{pm}. According to Table 7, the A_{pm} after the first treatment is larger than after the second cooling. Thus, the volume fraction of combeite in the samples becomes smaller after the second treatment.

Therefore, at the second crystallization peak occurred the transformation of combeite from a lower Na^+ content form crystallized at the lower temperature to a sodium-enriched one. In addition, in the second peak, the crystallization of devitrite takes place.

6.3 Devitrite crystallization

Figure 26 shows optical micrographs of C_2D cubic glass samples crystallized at 730 °C for different times, t. Combeite crystals formed a surface layer that grew perpendicular towards the center of the glassy sample. For t > 18 h, dendritic combeite crystallized in the bulk and was surrounded by residual glass after cooling. For t = 9 h and t = 21 h samples, XRD confirmed that only combeite formed before non-isothermal treatments (Figure 27). Thus, two morphologies of combeite crystals were crystallized.

Figure 26: Reflected optical micrography of the cross-section of cubic samples of C_2D glass heat-treated at 730 °C for a) 2.5 h, b) 17 h, c) 21 h and, d) amplification of the center of the sample treated for 21 h.

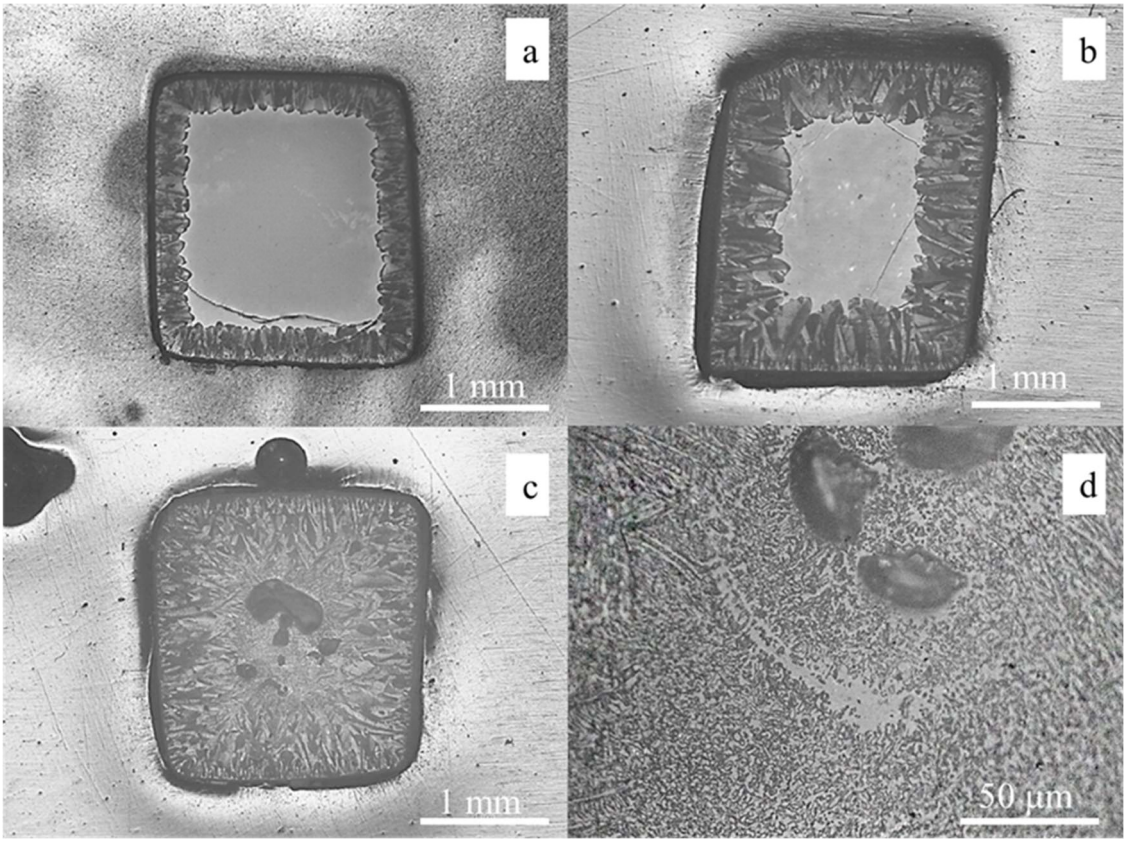

Source: Author (2021)

Figure 27: Diffractograms of cubic samples of C_2D glass (2 mm edge length) treated at 730 °C for a) 9 h and b) 21 h.

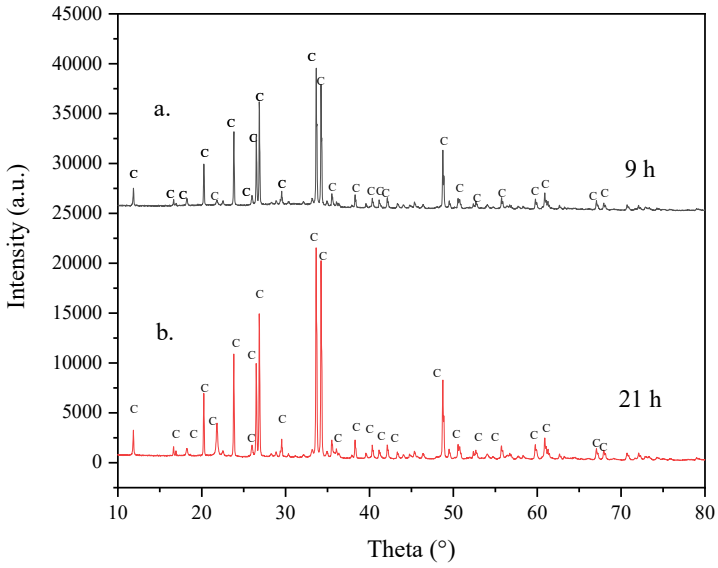

Source: Author (2021)

Figure 28 shows the DSC curves of cubic samples of C_2D glass previously treated for different times, t, (values of t are indicated in the figure). For the as-cast sample, T_g = 590 °C, and this value slightly decreased with the increase of heat-treatment time (Figure 29).

Figure 28: Cubic samples (2 mm length edge) of C_2D glass heat-treated at 730 °C for different times and subjected to non-isothermal treatment in a DSC and (a) heated from room temperature up to 1000 °C (10 °C/min), (b).polymorphic transition during cooling from 1000 °C (-10 °C/min) (c) detail of DSC of samples previously treated for t > 13 h.

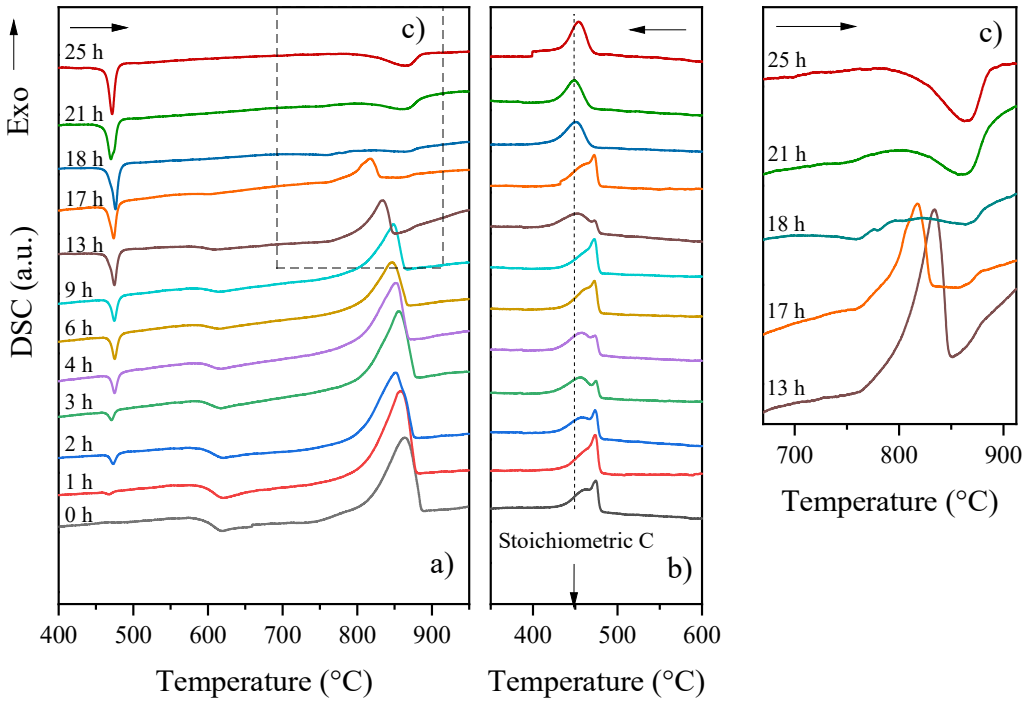

Source: Author (2021)

On heating, the endothermic peak due to the polymorphic transition of combeite previously crystallized only varies in intensity and was observed at ~470 °C regardless of the combeite volume fraction. Furthermore, based on the T_{pm} on heating, the composition of the dendritic combeite must be similar to the one in the surface layer and does not seem to change up to fully crystallization at t = 25 h. Thus, up to 730 °C, combeite is a solid solution with the composition of the parent glass.

Figure 29: T_{pm} of combeite and T_g of the residual glass of cubic C_2D samples isothermally treated at 730 °C for different intervals and subjected to non-isothermal treatment up to 1000 °C. T_{pm} and T_g were obtained from the heating DSC curve.

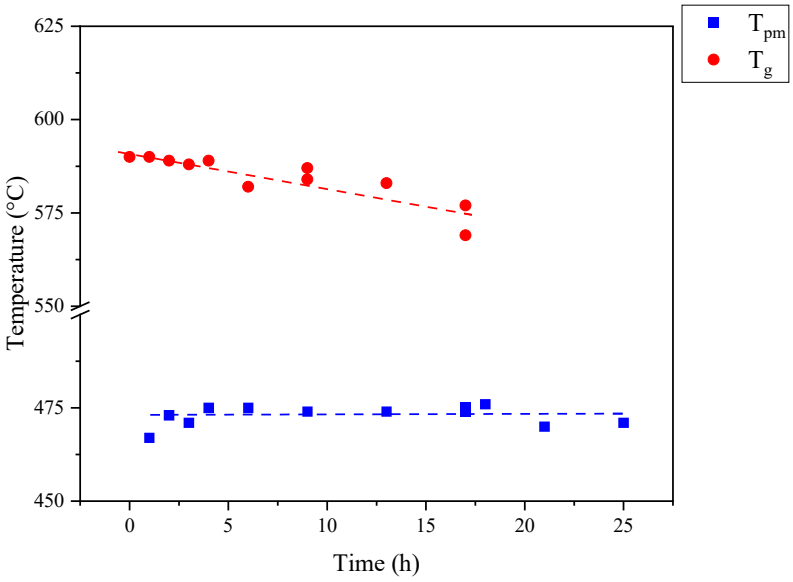

Source: Author (2021)

No exothermic reactions were observed during heating after lamellar combeite formation. For t > 18 h, an endothermic effect becomes evident above 810 °C and increases in intensity with the treatment time. One may suggest that this thermal event was overlapped by the crystallization peak in samples heat-treated for t < 17 h since they occur in the same temperature range. The endothermic peak that appears immediately after the endpoint of the crystallization for t = 13 h and t = 17 h may corroborate it, which is possibly the same peak observed for t > 18 h (Figure 28c). This thermal effect may correspond to the decomposition of a combeite solid solution.

Figure 30a shows an optical micrography of the cross-section of the sample previously treated for 21 h at 730 °C and non-isothermally treated up to 1000 °C at 10 °C/min. It is noticeable that the combeite surface layer was preserved in the sample. Also, a new eutectic phase crystallized in the center of the sample above 810 °C (Figure 30b). This microstructure was different from the one discussed above and consisted of alternating crystals of combeite and devitrite. However, it was not evident which area of Figure 30 corresponds to these phases.

Figure 30: (a) Optical micrography of the cross-section of C_2D sample previously treated at 730 °C for 21 h and submitted to a non-isothermal treatment up to 1000 °C (heating/cooling rate: 10 °C/min), and (b) detail of the eutectic microstructure formed in the center of the sample.

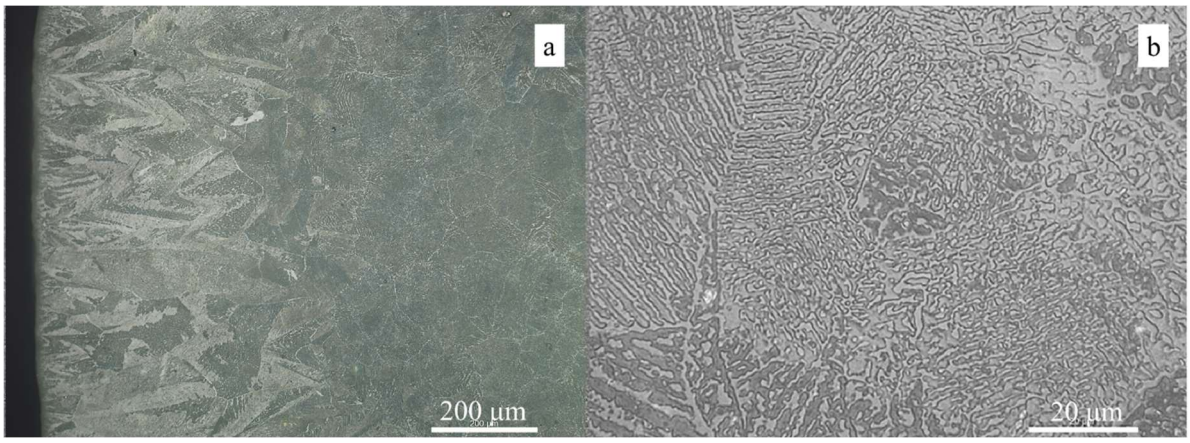

Source: Author (2021)

As shown in Figure 16, on heating, devitrite undergoes a peritectic reaction at 1030 °C [28]:

$$D \overset{1030\,^{\circ}C}{\longleftrightarrow} CS^{\beta} + Liquid \tag{10}$$

In this work, this transformation begins at T_s (Figure 13). It occurred at slightly higher temperatures for the C – D pseudo-binary and will be discussed in the next section.

The non-isothermal treatments were extended above T_S to observe whether this transformation occurs for the C_2D samples (Figure 31). The peritectic transformation of devitrite is indicated. According to this result, combeite and devitrite were crystallized throughout the treatments.

Figure 31: DSC curves (10 °C/min) of cubic C_2D samples treated at 730 °C for 4 and 25 h and subjected to non-isothermal treatment from room temperature up to 1250 °C (10 °C/min). The dashed line indicates the onset of the peritectic reaction.

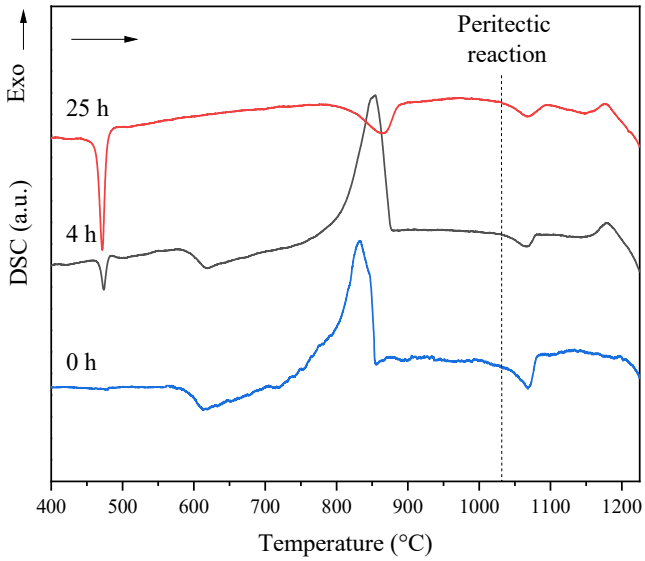

Source: Author (2021)

For partially crystallized glasses, two overlapped peaks due to the polymorphic transition were observed during cooling (Figure 28). The peak that appeared at higher temperatures was narrow and was immediately followed by a broad peak at lower temperatures. Similar behavior was described in the previous section. For t > 18 h, the polymorphic transition was observed on cooling as a single exothermic peak.

According to Figure 28b, for fully crystallized samples, T_{pm} on cooling shifted from higher temperatures to values close to the T_{pm} of the stoichiometric combeite (~450 °C). Here, one may suppose that at least part of the crystallized combeite behaved as a metastable phase since the sodium-depleted solid solution is not stable for T > 810 °C. Above this temperature, it partially disappears, and devitrite crystallizes. However, it was not clear if this process was a diffusional mechanism on solid-state or dissolution and reprecipitation of phases.

The crystallization of Cs.s. was not predicted for the equilibrium since combeite melting is a congruent reaction in the pseudo-binary studied in this work. However, Ostwald's Rule of Stages states that the primary phase to crystallize in a supercooled liquid is not necessarily the most stable [48]. Oppositely, the system can assume intermediate structural conformations, and each stage leads to a decrease in free energy. For instance, during the early stages of crystallization, metastable phases were reported for $Li_2O{\cdot}2SiO_2$ and $Na_2O{\cdot}2CaO{\cdot}3SiO_2$ glasses

[4,49]. For both glasses, the precipitation of solid solution was related to the decrease in the thermodynamical barrier to nucleation for the stable phase. In the case of $BaO{\cdot}2SiO_2$, monoclinic crystals, which are the high polymorphic structure, nucleate before the stable phase [50,51]. The stable polymorph at low temperatures was orthorhombic and only could be obtained by sample recrystallization. In [51], the $BaO{\cdot}2SiO_2$ metastable phase disappeared after non-isothermal treatments, likewise the ones performed in section 6.2.

Figure 32 shows samples of CD glass crystallized at 775 °C for different time intervals. The surface crystallization of CD samples began with the nucleation of combeite crystals, likewise C_2D glass. However, the crystallization of devitrite occurred at an earlier stage. As a result, devitrite crystallized internally to the glass but not homogenously (Figure 32d). In general, this phase presents heterogeneous nucleation and is known as a defect that grows on the surface of commercial soda-lime-silicate glasses [31,52]. The presence of combeite and devitrite was confirmed by diffractogram analysis (Figure 33).

Figure 32: Glass CD treated at 775 °C for a) 90 min, b) 150 min, c) 240 min; and d) is a zoom view of a devitrite crystal nucleated on the combeite surface in the sample treated for 150 min.

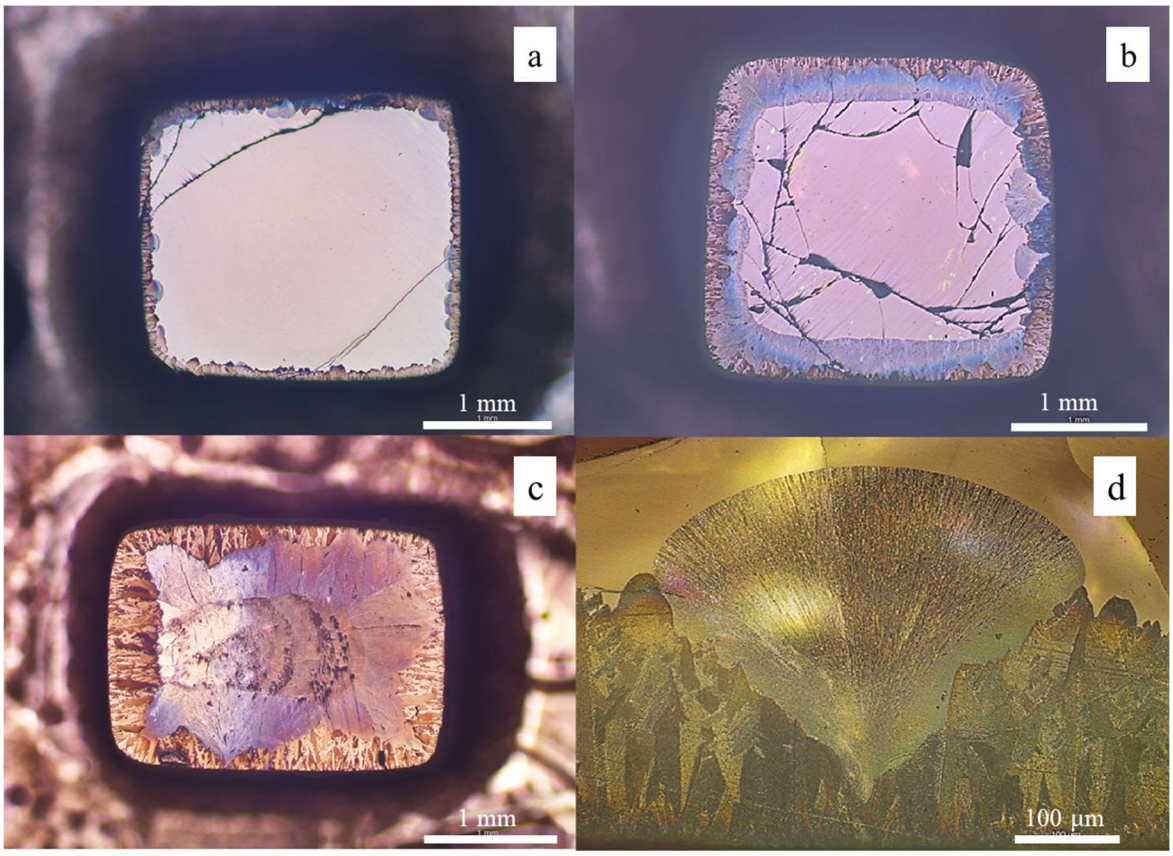

Source: Author (2021)

Figure 33: Diffractogram of CD glass heat-treated at 775 °C for 4h

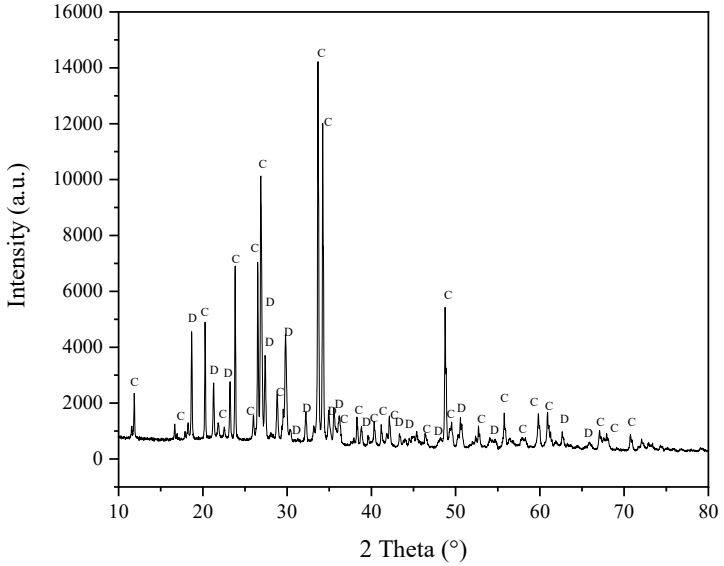

Source: Author (2021)

The growth of combeite formed diffusion zones depleted in sodium in the residual glass, which were observed as dark regions in the vicinity of the crystals in the EDS dot map (Figure 34). Diffusion zones are caused by the difference between the compositions of the parent glass and the growing crystals. Here, the surface of combeite crystals acts as nucleating sites for devitrite, and it crystallizes heterogeneously at the interface between combeite and the supercooled liquid (Figure 32d). As a result, the devitrite crystals grew parallel to the combeite layer and into the bulk of the glass. After the impingement of the devitrite crystals, the growth of the combeite crystals was hindered. The devitrite crystals continue to grow until fully crystallize the sample (Figure 32c).

Figure 34: EDS dot map with an overlay of Na of combeite layer in CD sample heat-treated at 775 °C for 120 min.

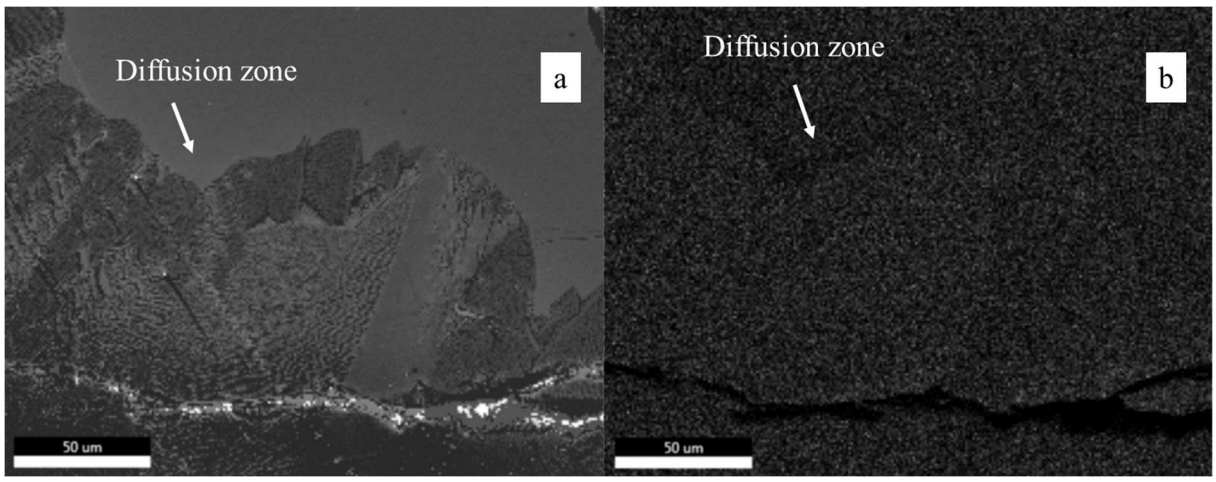

Source: Author (2021)

Besides the chemical composition change in the diffusion zone along the combeite interface, the stress arising from the difference between the densities of the residual glass and combeite crystals can lead to devitrite nucleation. This hypothesis was proposed due to the formation of several cracks in the vicinity of the crystalline layer (Figure 32). Table 8 shows the measured density of CD glass, ρ_{CD}, and the calculated densities of combeite, ρ_C, and devitrite, ρ_D, crystals.

Table 8: Densities of CD glass, combeite and devitrite crystals.

$\boldsymbol{\rho_{CD}}$ **(g/cm^3)**	$\boldsymbol{\rho_C}$ **(g/cm^3)**	$\boldsymbol{\rho_D}$ **(g/cm^3)**
2.70 [7]	2.82 [29]	2.71 [53]

Source: Macena *el al* (2020), Maki and Sugimura (1968) and IEM Databases and Datasets, Card No: 10288 (2020) [7,29,53]

The density misfit parameter, δ_d, that indicates the difference between ρ_{CD} and ρ_C is given by Eq. (11) and is proportional to the to the elastic stress energy originated during the crystallization [54,55]:

$$\delta_d = \frac{\rho_C - \rho_{CD}}{\rho_{CD}} \sim 0.044 \tag{11}$$

The stress-induced crystallization was found in stoichiometric diopside glasses ($CaO{\cdot}MgO{\cdot}2SiO_2$)[54]. For diopside $\delta_d = 0.160$ is a significant density variation between the crystals and the isochemical glass. Similar to the CD glass, diopside crystallization occurs by surface crystallization. Firstly, diopside crystals formed on the surface of a monolithic sample. As the diopside crystals impinge, the elastic stress energy produced by constricted diopside

crystallization leads to the crystallization of a second crystalline layer of wollastonite crystals. Wollastonite precipitated as a solid solution with density misfit parameter δ_d = 0.07. The formation of this second phase decreased the elastic energy stored in the sample due to its low density.

Additionally, the crystallization of the wollastonite layer terminates the crystallization of diopside. Therefore, although the density misfit parameter between combeite and CD glass was not high as observed for stoichiometric diopside, some resemblances can be suggested. For instance, the densities of CD glass and devitrite crystals are very close (δ_d = 0.004) (Table 8). Also, as mentioned before, the formation of the second crystalline layer stopped the combeite crystallization.

The compositional profile of CD glass heat-treated at 775 °C for 120 min was investigated by EDS (Figure 35). The combeite layer shows a different composition compared to the devitrite and the residual glass. Still, no compositional variation was identified between the devitrite and the glass or diffusion zone in residual glass. Since this sample presented a small volume fraction of combeite (Figure 32) at this stage of crystallization, the composition of the residual glass was analogous to the parent glass. Thus, devitrite may crystallize as a solid solution.

Figure 35: SEM BSE image and concentration (line scan) along the polished surface layer of cubic sample of CD glass (2 mm edge length) heat-treated at 775 °C for 120 min. 1, 2 and 3 show the glass, devitrite crystal and combeite layer, respectively.

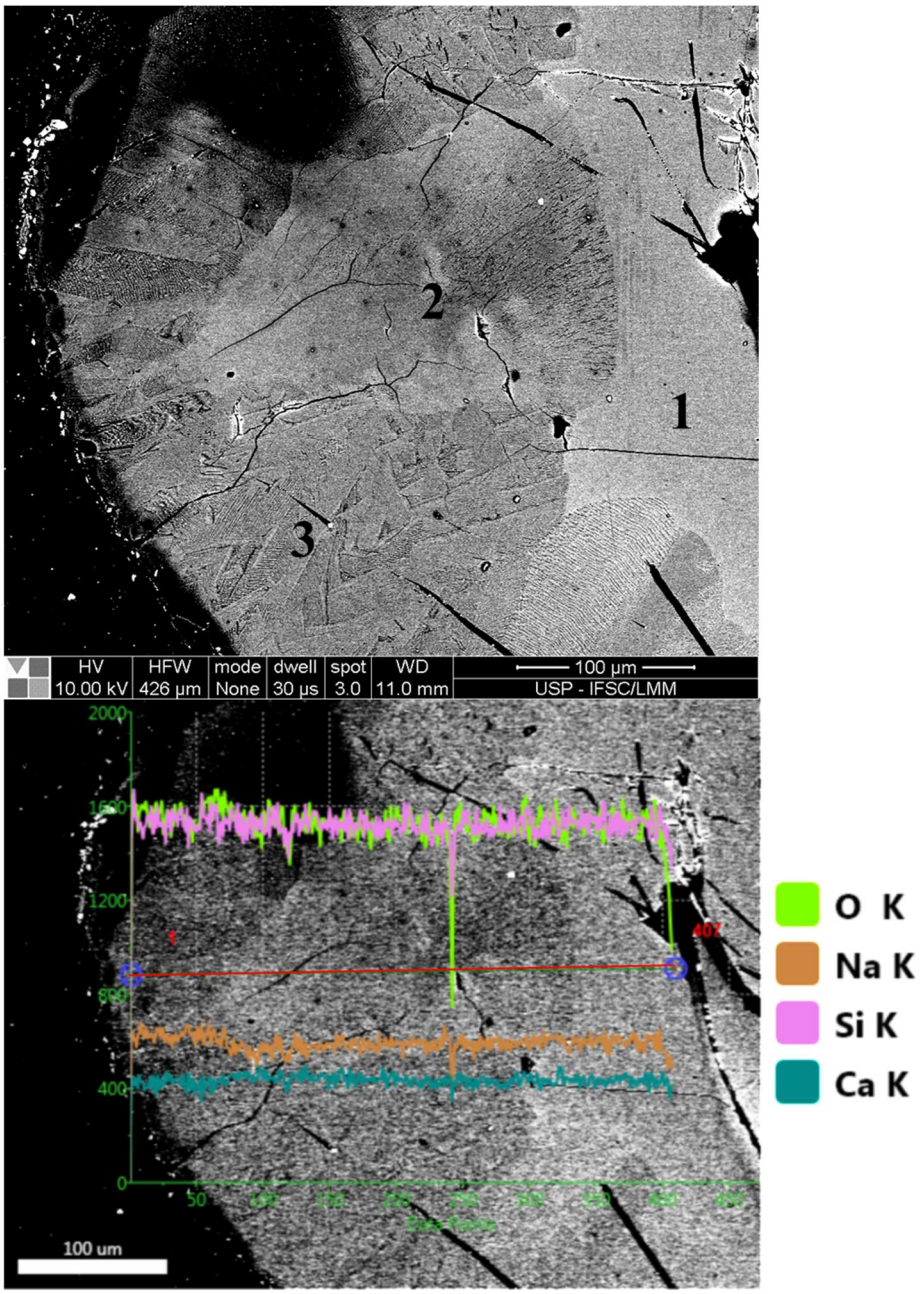

Source: Author (2021)

6.4 Crystallization at temperatures between T_S and T_L

Figure 36 shows the cross-section sample of C_2D and CD glasses treated at 1100 °C for 20 and 90 min, respectively, i.e., between 1050 °C and 1260 °C, approximately T_S and T_L of these compositions (Figure 13), immediately after melting at 1350 °C. Again, a glassy matrix

surrounded the dendritic crystals. According to the phase diagram (Figure 17), three phases exist in equilibrium for samples of both glasses at 1100 °C: β-wollastonite, combeite, and liquid.

Figure 36: Reflected light optical micrography along the polished surface layer of glasses: (a, b) C_2D heat-treated at 1350 °C for 20 min and then 1100 °C for 15 min and (c, d) CD treated at 1350 °C for 20 min and 1100 °C for 90 min

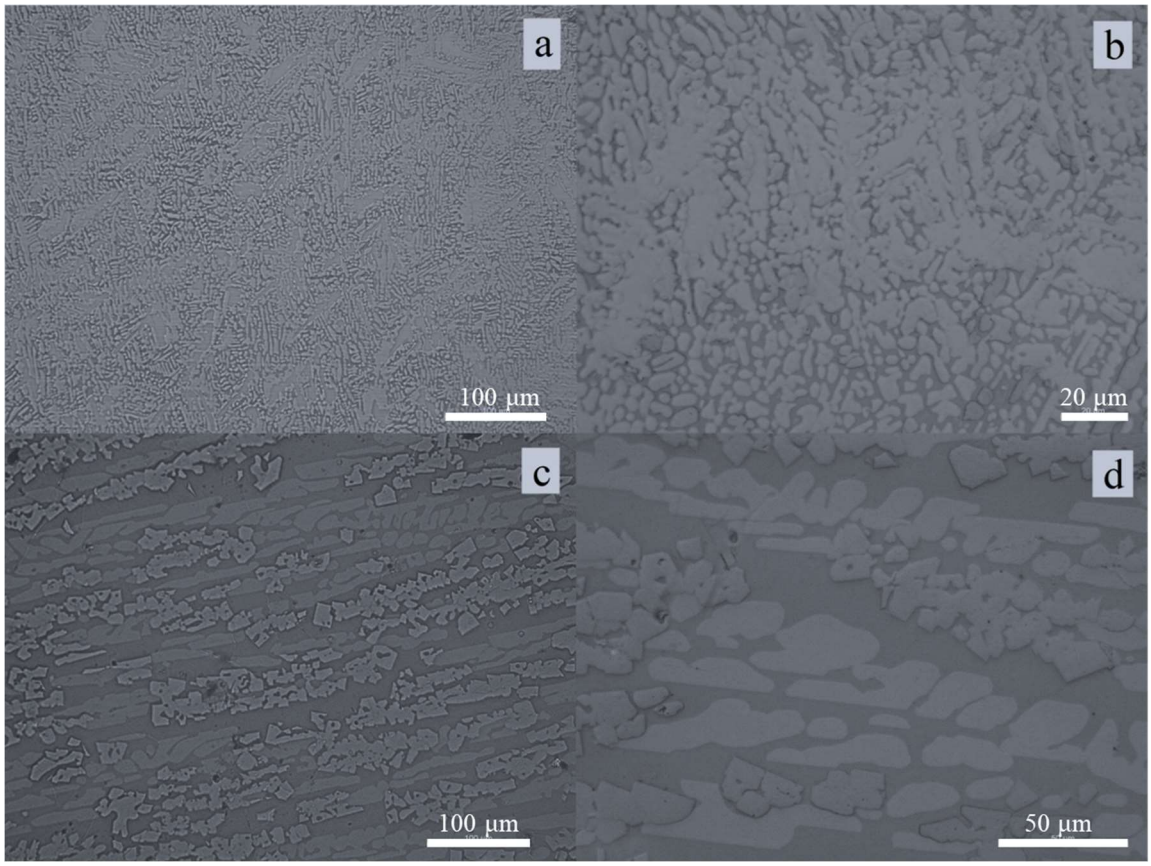

Source: Author (2021)

The concentration of the elements Na, Ca, Si and O in the C_2D was examined across the width (line scan) of the C_2D sample (Figure 37). The compositional variation evidenced three phases.

Figure 37: SEM BSE image and concentration along the polished surface layer of C_2D glass heat-treated at 1350 °C for 10 min and then 1100 °C for 20 min

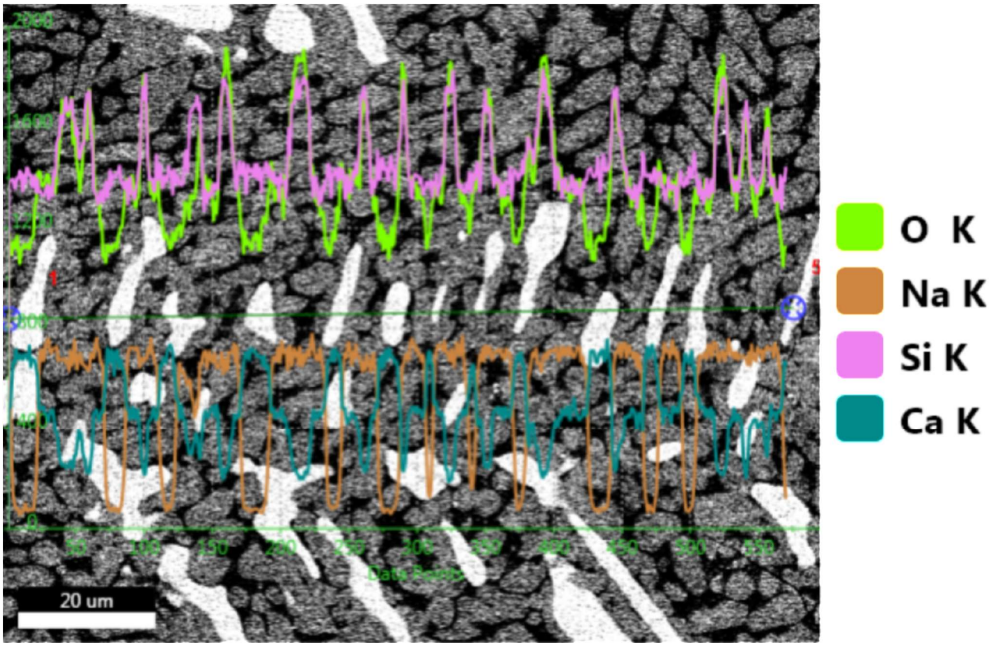

Source: Author (2021)

Table 9: Composition (wt%) of the phases formed in C_2D composition after heat-treatment at 1350 °C for 10 min and then 1100 °C for 20 min measured by EDS and the nominal compositions (wt%) of combeite, wollastonite and, C_2D glass.

		Composition measured by EDS (wt%)			Nominal composition (wt%)		
		Grey	White	Black	Combeite	Wollastonite	C_2D
Element	O	36 ± 8	38.2 ± 0.2	42 ± 8	40.63	41.32	41.86
	Na	14.5 ± 0.2	0.1 ± 0.2	13.3 ± 0,7	12.97	-	10.62
	Si	23 ± 2	22.8 ± 0.1	33.6 ± 4	23.78	24.18	25.94
	Ca	26 ± 6	38.9 ± 0.2	12 ± 3	22.62	34.50	21.59

Source: Author (2021)

Although the chemical contrast shown in Table 9 does not correspond to absolute values, it suggested that the grey, white, and black phases Figure 37 were combeite, wollastonite, and a glassy matrix, respectively. The surface layer of the treated sample was subjected to XRD, confirming the presence of combeite and β-wollastonite (Figure 38).

Figure 38: Driffractogram of C_2D glass treated at 1350 °C for 10 min and immediately treated at 1100 °C for 20 min.

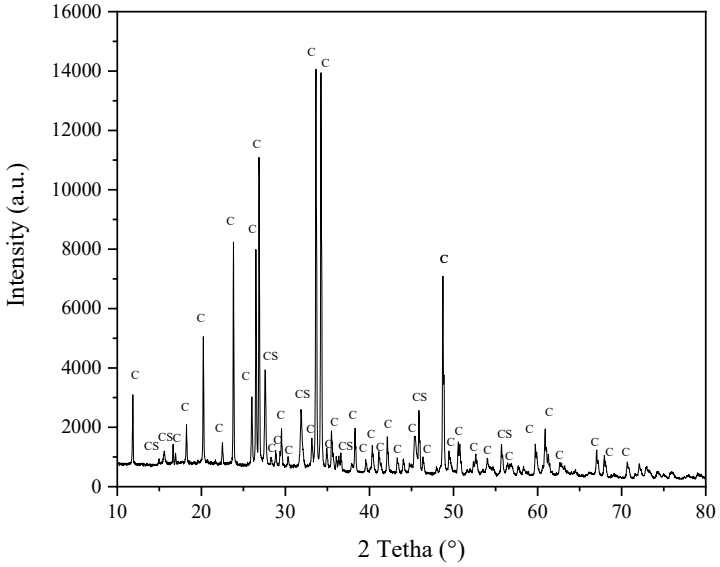

Source: Author (2021)

A powdered sample of the stoichiometric D glass was heat-treated at 1100 °C for 72 h (Figure 39). The sample showed a background corresponding to residual glass and crystallized only β-wollastonite according to the diffractogram analysis.

Figure 39: Diffractogram of D glass heat-treated at 1100 °C for 72 h with Si as internal reference pattern.

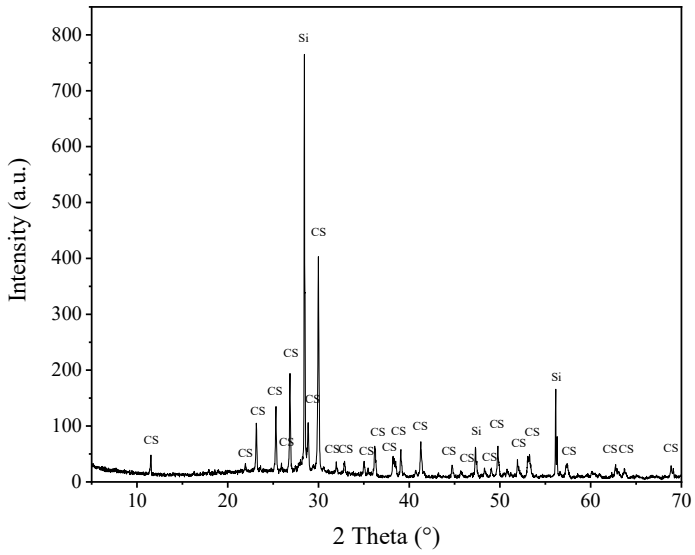

Source: Author (2021)

Therefore, the endothermic peak with onset at T_s (Figure 13 and Figure 31) corresponds to the peritectic reaction at which devitrite forms β-wollastonite and liquid on heating. The peritectic transformation temperatures of the glasses in this work are summarized in Table 6. The T_s values were higher than the 1030 °C presumed in Figure 16. However, Maki and Morey reported that stoichiometric devitrite would decompose to β-wollastonite and liquid at 1045 °C and 1060 °C, respectively, which are closer to the temperatures found [56,57].

6.5 Formation of solid solution

C, $C_{15}D$, C_7D, C_3D and, C_2D glasses were crystallized by the Tammann method, as summarized in Table 5. According to the XRD patterns, only combeite was formed in these compositions. The behavior of the lattice parameters *a* and *c* of combeite are shown in Figure 40. Since the samples were fully crystallized, the crystals present the same average composition as the parent glass. Compositions with sodium content below 13.6 mol% did not show homogeneous nucleation in laboratory time scales.

Figure 40: Dependence of the hexagonal unit cell parameters of combeite as a function of the parent glass composition.

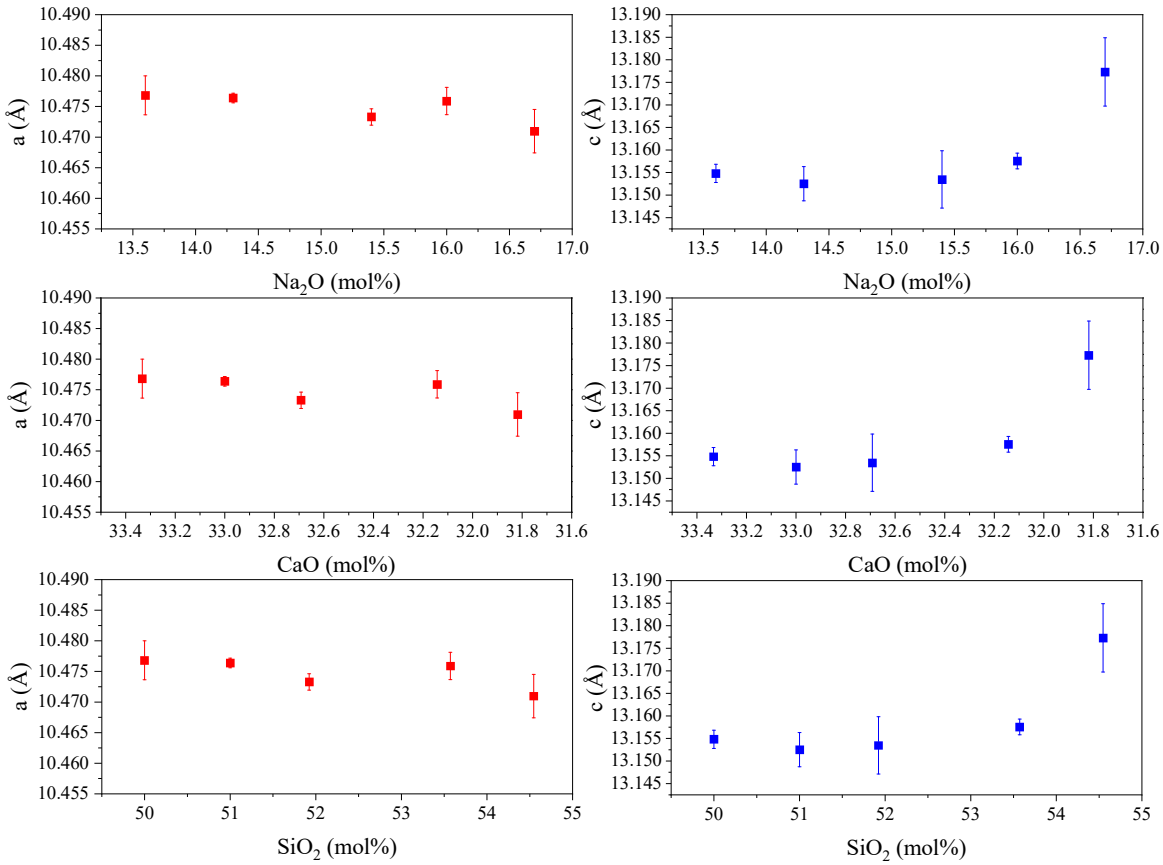

Source: Author (2021)

Stoichiometric combeite hexagonal crystal parameters presented values of $a = 10.471 \pm 0.004$ Å and $c = 13.177 \pm 0.008$ Å, which coincide with the literature [29]. The mean values of *a* are not significantly different. On the other hand, parameter *c* decreases with the sodium concentration in the parent glass, notably between compositions C and C_7D (16.7 and 15.84 mol% Na_2O). The variation of this parameter may indicate the formation of combeite in solid solution.

In [4], during the crystallization of stoichiometric combeite glass, the amount of sodium in the crystals was greater at the begging of the crystallization than in the parent glass. As crystals grow, this difference in composition between crystal and glass tends to vanish due to the lower availability of sodium ions in the vicinity of the crystal. Thus, the combeite crystals present a sodium concentration gradient as a function of the diameter: the closer to the center of the crystal, the greater the sodium concentration. On the other hand, the content of Ca^{2+} ions

shows an opposite behavior. At BSE images, regions enriched in havier atoms are brighter when compared to ones that present less of these elements. Thus, one may expect that the vicinity of the crystal would be bright, whereas the center of the crystal dark and getting lighter towards its edge. Figure 41 shows SEM BSE image of C_2D glass heat-treated at 582 °C for 120 h and 700 °C for 60 min. Neither diffusion zones at the vicinity of the crystal nor changes of composition in the crystal were detected in this analysis (Figure 41).

Figure 41: SEM BSE image of C_2D glass heat-treated at T_n = 582 °C/120 h + T_d = 700 °C/60 min

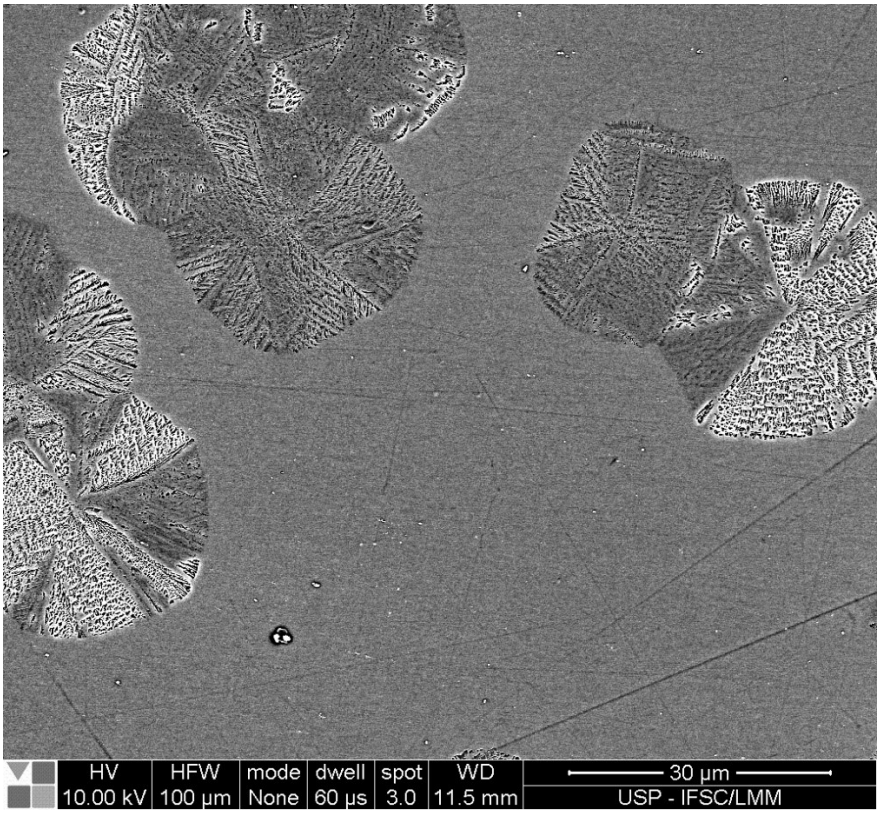

Source: Author (2021)

Figure 42: **EDS dot map with overlay of Na of glass C_2D heat-treated at T_n = 582 °C/120 h + T_d = 700 °C/60 min.**

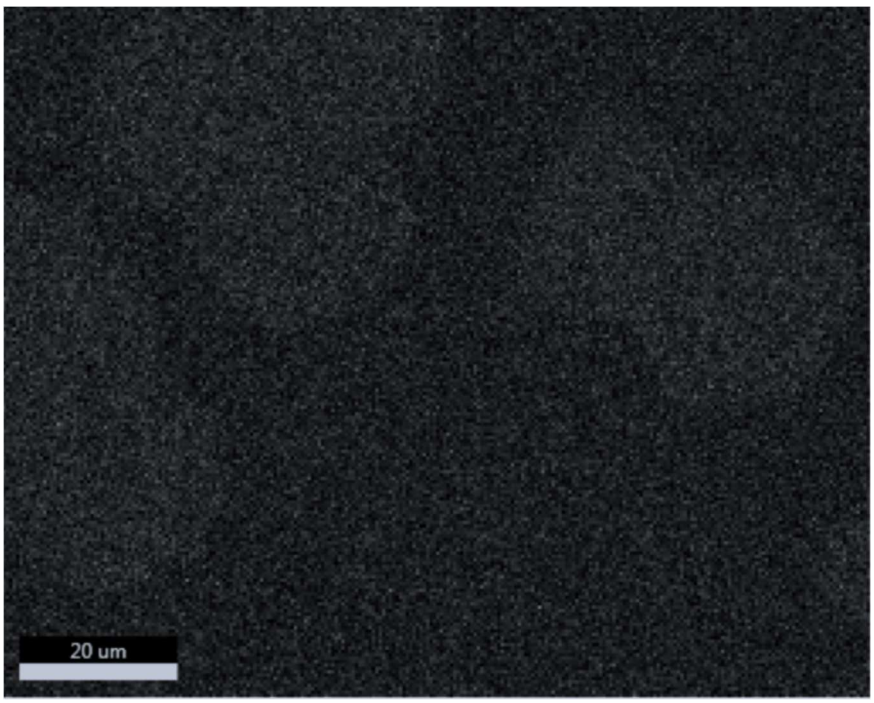

Source: Author (2021)

However, the EDS dot map of this sample (Figure 42) showed that combeite crystals presented a higher Na content than the residual glass. As mentioned before, fully crystallized samples of C_2D glass presented only combeite. Therefore, the amount of sodium in the crystal diminishes with the increase in its diameter. Also, according to Figure 43, crystals nucleated in the surface of the sample's present compositional variation: the crystal growth is accompanied by a decrease of Na content.

Figure 43: EDS line profile of the cross section parallel to the surface of glass C_2D heat-treated at T_n = 582 °C/120 h + T_d = 700 °C/60 min

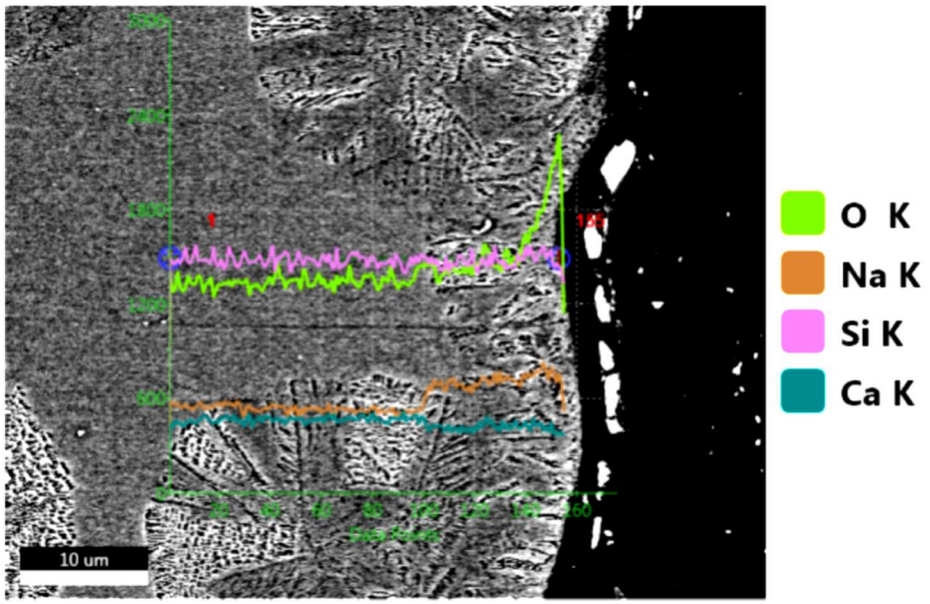

Source: Author (2021)

Fokin *et al.* and Soboleva *et al.* reported that the formation of combeite solid solution in soda-lime glasses is accompanied by an increase in parameter *a* with the Na content increase [4,5]. Figure 44 shows *a* parameter as a function of the Na_2O content for fully crystallized glasses. As mentioned before, the modification in the combeite crystalline network is a consequence of exchanging one Ca^{2+} for two Na^{+}, which forms a continuous series of $Na_{4+2x}Ca_{4-x}[Si_6O_{18}]$ solid solutions. However, these authors studied compositions close to the metasilicate section or at the metasilicate join (Na_2SiO_3 - $CaSiO_3$).

Figure 44: Dependence of a parameter as a function of Na_2O content in the parent glass for fully crystallized glasses.

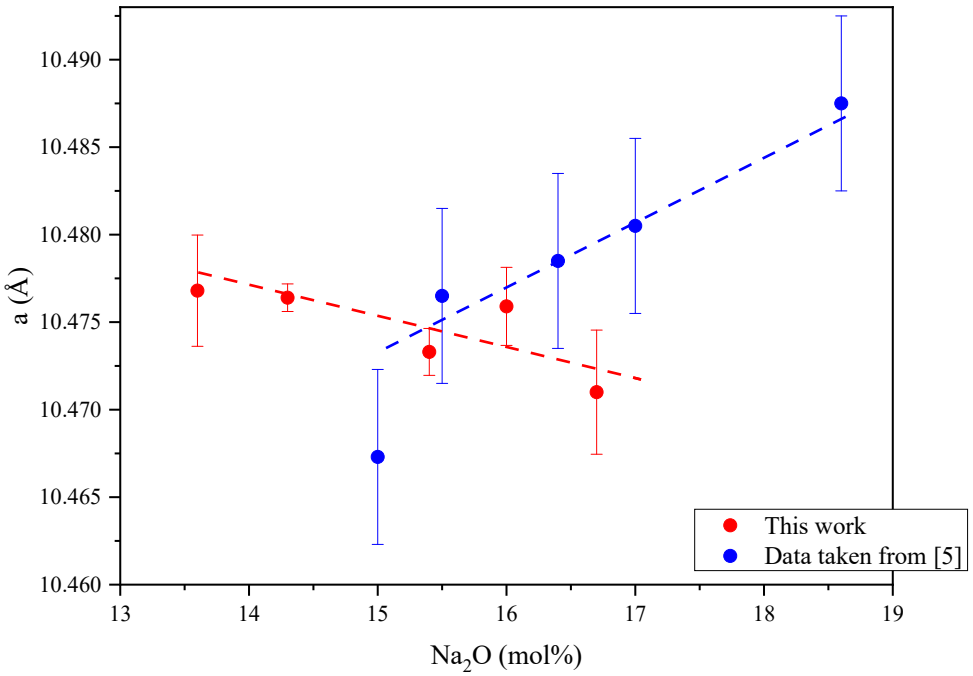

However, according to Figure 40, the lattice parameter variation was observed in the *c* axis. Also, the dependence of the *c* parameter as a function of sodium content was not linear. In this work, the proportion of silicon oxide increased systematically. Therefore, this simple ion exchange could not explain the variation of the parameters in their entirety, and more complex solid solutions may occur. In fact, for some solid solutions, the introduction of cations within the lattice forces displacements in the host structure, causing deviations of the linear dependence between the crystal parameters and composition [58,59]. Further investigations are required.

7 CONCLUSION

This work investigated the phases formed in glasses in the $Na_2O{\cdot}2CaO{\cdot}3SiO_2$–$Na_2O{\cdot}3CaO{\cdot}6SiO_2$ pseudo-binary system after isothermal and non-isothermal treatments.

In the assessment of glasses with composition between 0 and 50 mol% D, combeite was the kinetically preferred phase even for CD glass that undergoes only surface crystallization.

Combeite and devitrite were identified in C_2D and CD glasses after non-isothermal treatments in DSC. This occurrence is consistent with the equilibrium phase diagram. In both glasses, it was observed two combeite types in terms of sodium content. After treatments up to the first crystallization peak shown in DSC, combeite was crystallized as a solid solution. This phase presented less sodium and a smaller compositional gradient than the combeite formed in the second crystallization peak. Also, the combeite volume fraction decreased during the non-isothermal treatments up to the second peak. The crystallization of devitrite accompanied the decomposition of combeite solid solution.

Thus, it is suggested that the combeite solid solution was metastable against the stoichiometric one. This transformation does not occur up to 810 °C for C_2D glass. The precipitation of this solid solution decreases the thermodynamical barrier to the crystallization of devitrite.

Lamellar combeite and wollastonite in a matrix of residual glass were obtained by slow colling from T_L samples of C_2D and CD compositions and isothermally treating them above T_S. It was confirmed that T_S corresponded to the onset of the peritectic reaction of devitrite. Stoichiometric D glass also crystallized wollastonite after isothermal treatment at the same temperature.

The occurrence of combeite solid solution. was investigated by XRD in the hypo-eutectic section of the binary (less than 33.3 mol% of D). The variation of the lattice parameter *c* of combeite crystal suggests the formation of combeite solid solution in the interval between 0 and 33.33 mol% of D. This relation between the *c* parameter and the content of Na_2O was never reported. A distinct solid solution may be formed due to the variation in the proportion of SiO_2 in the parent glasses.

8 FOR FUTURE INVESTIGATION

- To study the mechanism of crystallization of devitrite in glasses with composition 33.33 and 50 mol% D.
- To investigate the combeite solid solution structure formed in glasses with composition between 0 and 33.33 mol% D.

REFERENCES

[1] GONZÁLEZ OLIVER, C. J. R. **Crystal Nucleation and Growth in Soda-Lime-Silica Glasses**. 1979. 1–385 f. University of Sheffield. 1979.

[2] GONZÁLEZ OLIVER, C. J. R.; JAMES, P. F. Crystal nucleation and growth in soda-lime-silica glasses close to the Na2O·2 CaO·3 SiO2(NC2S3) composition. Crystal nucleation kinetics in the stoichiometric NC2S3 composition. **Thermochimica Acta**, v. 280–281, n. SPEC. ISS., p. 223–236, 1996.

[3] FOKIN, V. M.; ZANOTTO, E. D. Continuous compositional changes of crystal and liquid during crystallization of a sodium calcium silicate glass. **Journal of Non-Crystalline Solids**, v. 353, n. 24–25, p. 2459–2468, 2007.

[4] FOKIN, V. M. et al. Mutant crystals in Na2O · 2CaO · 3SiO2 glasses. **Journal of Non-Crystalline Solids**, v. 331, n. 1–3, p. 240–253, 2003.

[5] SOBOLEVA, E. N.; YURITSYN, N. S.; UGOLKOV, V. L. Kinetics of Crystal Nucleation of Na 2 O · 2CaO · 3SiO 2 -Based Solid Solutions in Glasses of the Na 2 SiO 3 – CaSiO 3 Pseudobinary Join. **Glass Physics and Chemistry**, v. 30, n. 6, p. 481–486, 2004.

[6] MACENA, G. DA S. **Cinética de cristalização não-estequiométrica de vidros no Sistema Na2O.2CaO.3SiO2 – Na2O.3CaO.6SiO2**. 2019. Universidade de São Paulo. 2019.

[7] MACENA, G. S. et al. Off-stoichiometry effects on crystal nucleation and growth kinetics in soda-lime-silicate glasses. The combeite (Na2O•2CaO•3SiO2) – devitrite (Na2O•3CaO•6SiO2) joint. **Acta Materialia**, v. 196, p. 191–199, 2020.

[8] ZANOTTO, E. D.; MAURO, J. C. The glassy state of matter: Its definition and ultimate fate. **Journal of Non-Crystalline Solids**, v. 471, n. March, p. 490–495, 2017.

[9] SCHERER, G. W. Relaxation in glass and composites. 1986.

[10] DONTH, E. **The glass transition: relaxation dynamics in liquids and disordered materials**. [s.l.] Springer Science & Business Media, 2013. v. 48

[11] KELTON, K. F.; GREER, A. L. The classical theory. In: **Pergamon Materials Series**. [s.l.] Elsevier, 2010. v. 15p. 19–54.

[12] SCHMELZER, J. W. P. et al. Effects of glass transition and structural relaxation on crystal nucleation: Theoretical description and model analysis. **Entropy**, v. 22, n. 10, p. 1098, 2020.

[13] FOKIN, V. M. et al. Effect of structural relaxation on crystal nucleation in glasses. **Acta Materialia**, v. 203, p. 116472, 2021.

[14] ZANOTTO, E. D. A bright future for glass-ceramics. **Journal of the American Ceramic Society**, v. 89, n. 8, p. 19–27, 2010.

[15] LEWIS, M. H. **Glasses and glass-ceramics**. [s.l.] Springer Science & Business Media, 2013.

[16] TURNBULL, D.; FISHER, J. C. Rate of nucleation in condensed systems. **The Journal of chemical physics**, v. 17, n. 1, p. 71–73, 1949.

[17] CHRISTIAN, J. W.; JW, C. The theory of transformations in metals and alloys. I. Equilibrium and general kinetic theory. 1975.

[18] ABYZOV, A. S.; FOKIN, V. M.; ZANOTTO, E. D. Predicting homogeneous nucleation rates in silicate glass-formers. **Journal of Non-Crystalline Solids**, v. 500, n. August, p. 231–234, 2018.

[19] ZANOTTO, E. D. Isothermal and adiabatic nucleation in glass. **Journal of Non-Crystalline Solids**, v. 89, n. 3, p. 361–370, 1987.

[20] MÜLLER, R.; ZANOTTO, E. D.; FOKIN, V. M. Surface crystallization of silicate glasses: Nucleation sites and kinetics. **Journal of Non-Crystalline Solids**, v. 274, n. 1, p. 208–231, 2000.

[21] UHLMANN, D. R. CRYSTAL GROWTH IN GLASS-FORMING SYSTEMS: A TEN-YEAR PERSPECTIVE. In: **Advances in ceramics**. [s.l.] American Ceramic Soc Inc, 1982. p. 80–124.

[22] HÖLAND, W.; BEALL, G. **Glass-ceramic Technology**. Second ed. [s.l.] John Wiley & Sons, Inc., Hoboken, New Jersey, 2012.

[23] MAURO, J. C. et al. Glass science in the United States: Current status and future directions. **International Journal of Applied Glass Science**, v. 5, n. 1, p. 2–15, 2014.

[24] MAURO, J. C.; ZANOTTO, E. D. Two Centuries of Glass Research: Historical Trends, Current Status, and Grand Challenges for the Future. **International Journal of Applied Glass Science**, v. 5, n. 3, p. 313–327, 2014.

[25] KOKUBO, T. et al. Formation of a high-strength bioactive glass-ceramic in the system MgO-CaO-SiO2-P2O5. **Journal of Materials Science**, v. 21, n. 2, p. 536–540, 1986.

[26] SOARES, V. O. et al. New sintered wollastonite glass-ceramic for biomedical applications. **Ceramics International**, v. 44, n. 16, p. 20019–20027, 2018.

[27] FOKIN, V. M.; ZANOTTO, E. D.; SCHMELZER, J. W. P. Homogeneous nucleation versus glass transition temperature of silicate glasses. **Journal of Non-Crystalline Solids**, v. 321, n. 1–2, p. 52–65, 2003.

[28] SHADID, K. A,; GLASSER, F. P. Phase equilibria in the glass forming region of the system Na2-CaO-MgO-SiO2. **Physics and Chemistry of Glasses**, v. 13, n. 2, p. 27–42, 1972.

[29] MAKI, I.; SUGIMURA, T. **Metasilicates in Ternary System Na2O-CaO-SiO2**NagoyaJ. Ceram. Assoc. Japan, , 1968.

[30] MOREY, G. W.; BOWEN, N. L. Devitrite. **The Glass Industry**, v. 12, n. 6, p. 133, 1931.

[31] KNOWLES, K. M.; THOMPSON, R. P. Growth of devitrite, Na 2 Ca 3 Si 6 O 16, in soda-lime-silica glass. **Journal of the American Ceramic Society**, v. 97, n. 5, p. 1425–1433, 2014.

[32] BUTT, H. et al. Devitrite-Based Optical Di ff users. n. 3, p. 2929–2935, 2014.

[33] BUTT, HAIDER; KNOWLES, K. **Optical diffuser containing devitrite**Great Britain, 2015.

[34] LI, H.; CHANG, J. Preparation, characterization and in vitro release of gentamicin from PHBV/wollastonite composite microspheres. **Journal of Controlled Release**, v. 107, n. 3, p. 463–473, 2005.

[35] KOKUBO, T. Bioactive glass ceramics: properties and applications. **Biomaterials**, v. 12, n. 2, p. 155–163, 1991.

[36] HING, K. A. et al. Effect of silicon level on rate, quality and progression of bone healing within silicate-substituted porous hydroxyapatite scaffolds. **Biomaterials**, v. 27, n. 29, p. 5014–5026, 2006.

[37] XIONG, K. et al. Control of the dissolution of Ca and Si ions from CaSiO 3 bioceramic via tailoring its surface structure and chemical composition. **Journal of the American Ceramic Society**, v. 96, n. 3, p. 691–696, 2013.

[38] NURJAYA, D. M.; ASTUTININGSIH, S.; ZULFIA, A. Thermal effect on flexural strength of geopolymer matrix composite with alumina and wollastonite as fillers. **International Journal of Technology**, v. 6, n. 3, p. 462–470, 2015.

[39] OHSATO, H.; TAKÉUCHI, Y.; MAKI, I. Structural study of the phase transition of Na4Ca4[Si6O18]. **Acta Crystallographica Section B**, v. 46, n. 2, p. 125–131, 1990.

[40] OHSATO, H.; MAKI, I.; TAKÉUCHI, Y. Structure of Na2CaSi206. **Acta Crystallographica**, v. C41, n. Table l, p. 1575–1577, 1985.

[41] OHSATO, H.; TAKÉUCHI, Y.; MAKI, I. Structure of Na4Ca4[Si6O18]. **Acta Crystallographica**, v. C42, p. 934–937, 1986.

[42] VEGARD, L. Die konstitution der mischkristalle und die raumfüllung der atome. **Zeitschrift für Physik**, v. 5, n. 1, p. 17–26, 1921.

[43] FOKIN, V. M. et al. Effect of pre-existing crystals on the crystallization kinetics of a soda-lime-silica glass. The courtyard phenomenon. **Journal of Non-Crystalline Solids**, v. 258, n. 1, p. 180–186, 1999.

[44] POTAPOV, O. V. et al. Influence of Na2O content on the nucleation kinetics in glasses of compositions close to the Na2O · 2CaO · 3SiO2 stoichiometry. **Glass Physics and Chemistry**, v. 26, n. 2, p. 27–32, 2000.

[45] TAMMANN, G. Ueber die abhangkeit der Zahl der Kernr, welche sich in verschiedenen underkuhlten flusflussigkeiten. **Z Phys Chem**, v. 25, p. 441–479, 1898.

[46] FOKIN, V. M. et al. Homogeneous crystal nucleation in silicate glasses : A 40 years perspective. **Journal of Non-Crystalline Solids**, v. 352, p. 2681–2714, 2006.

[47] ZANOTTO, E. D. Glass Crystallization Research - A 36-Year Retrospective. Part I, Fundamental Studies. **International Journal of Applied Glass Science**, v. 4, n. 2, p. 105–116, 2013.

[48] OSTWALD, W. Lehrbuch der Allgemeinen Chemie, vol. 2; W. Engelmann: Leipzig, Germany, 1896; p 444. Ostwald, W. **Z. Phys. Chem**, v. 22, p. 289–330, 1897.

[49] DEUBENER, J.; BRÜCKNER, R.; STERNITZKE, M. Induction time analysis of nucleation and crystal growth in di- and metasilicate glasses. **Journal of Non-Crystalline Solids**, v. 163, n. 1, p. 1–12, 1993.

[50] LEWIS, M. H.; SMITH, G. Spherulitic growth and recrystallization in barium silicate glasses. **Journal of Materials Science**, v. 11, n. 11, p. 2015–2026, 1976.

[51] ARAUJO, M. C. C. et al. Residual glass and crystalline phases in a barium disilicate glass-ceramic. **Materials Characterization**, v. 110, p. 192–196, 2015.

[52] HRMA, P. et al. Effect of float glass composition on liquidus temperature and devitrification behaviour. **Glass Technology-European Journal of Glass Science and Technology Part A**, v. 47, n. 3, p. 78–90, 2006.

[53] **IEM Databases and Datasets, Card No: 10288.** , [s.d.].

[54] FOKIN, V. M. et al. Stress induced pore formation and phase selection in a crystallizing stretched glass. **Journal of Non-Crystalline Solids**, v. 356, n. 33–34, p. 1679–1688, 2010.

[55] SCHMELZER, J. et al. Surface-induced devitrification of glasses: the influence of elastic strains. **Journal of Non-Crystalline Solids**, v. 162, n. 1–2, p. 26–39, 1993.

[56] MOREY, G. W. The devitrification of soda-lime-silicate. v. 226, n. 9, 1930.

[57] MAKI, I. Unit Cell Data for Devitrite, Na2Ca3Si6O16. **Journal of the Ceramic Association, Japan**, v. 76, n. 6, p. 33–34, 1967.

[58] ALLEN, G. C.; HALLAM, K. R. X-ray diffraction studies of solid solutions of Cr-, Mn-, Fe-, Co-,and Ni-containing transition metal spinel oxides. **Powder Diffraction Journal**, v. 26, n. 3, p. 214–220, 1995.

[59] KUZMIN, A.; MIRONOVA, N. Composition dependence of the lattice parameter in NicMg1-cO solid solutions. **Journal of Physics Condensed Matter**, v. 10, n. 36, p. 7937–7944, 1998.